University of Nevada, Reno

Development of Mobile Solar Evaluation Laboratory & Technical and Economic Performance of the Goldade Site-Built Air Collector

A thesis submitted in partial fulfillment
of the requirements for the degree of Masters of Science
Mechanical Engineering

by

Travis D. Goldade

Dr. Cahit A. Evrensel/Thesis Advisor

December, 2015

THE GRADUATE SCHOOL

We recommend that the thesis
prepared under our supervision by

TRAVIS D. GOLDADE

entitled

Development Of Mobile Solar Evaluation Laboratory & Technical And Economic Performance Of The Goldade Site-Built Air Collector

be accepted in partial fulfillment of the
requirements for the degree of

MASTER OF SCIENCE

Cahit A. Evrensel, Ph.D., Advisor

Robert H. Turner, Ph.D., Committee Member

S. Kent Hoekman, Ph.D., Graduate School Representative

David W. Zeh, Ph.D., Dean, Graduate School

December, 2015

Abstract

The Great Basin climate type is ideal for the utilization of solar winter space heat from air collectors; perhaps the most economically viable option for solar space heating is that of site built air collectors (SBAC). Unfortunately SBACs are a rarely utilized technology primarily because there is presently no standard method to test these types of collectors. This thesis provides a viable testing method for SBACs and the theoretical calculations required to develop testing and provide ratings based on industry standards. This leads to development of the Mobile Solar Evaluation Laboratory (MSEL).

The Goldade Family built a 128 ft^2 solar air heater for winter space heating, and the MSEL was employed to evaluate the technical and economic performance of that system. Theory and field testing correlated well, and it was proven that the MSEL accurately predicts SBAC performance. In most Northern Nevada households solar space heating can be cost effective. Solar space heating also reduces substantial CO_2 from being added to the atmosphere.

Acknowledgements

The thesis would not have been possible without the help and support from both my parents in the financing and construction of the SBAC located at their home. Nor would have any of this been possible without the help and guidance from my friend and mentor Bob Turner. Finally Curt Robbins and Sean Sullivan helped with the design and construction of the MSEL unit.

Table of Contents

Chapter 1. Site Built Air Collectors (SBAC) 5
Previous Work 11
Chapter 2. Incentives & SRCC Standards for Solar Air Heaters 14
Chapter 3. Replicating SRCC Standards in the Field for Site Built Air Collectors 19
Hand-Held Velocity Meter Mathematical Development 30
Sensitivity Test 33
Chapter 4. Development of a Mobile Solar Evaluation Laboratory (MSEL) 37
Measuring Flow Rate 44
MSEL Set-Up & Data Handling 51
Chapter 5. Field Testing and Validation of the (MSEL) on Goldade Collector 55
Goldade Collector Theoretical Analysis 55
Technical Evaluation using the MSEL 73
Chapter 6. System Description and Cost 78
Chapter 7. Economic Performance of the Goldade Solar System 89
f-Chart Estimate of the Goldade System 89
Economic Performance of the Goldade System: 102
Carbon Dioxide Mitigation 106
Chapter 8. Summary, Results and Conclusion 108

List of Tables

Table 3-1: Error List for a Venturi Nozzle 36
Table 3-2: Error List for Hand Held Flow Meter 36
Table 5-1: Collector Dimensions 59
Table 5-2: h_r versus T_{Ave} 69
Table 5-3: Comparing Theoretical to Field Test Parameter Values for the Goldade Collector 77
Table 6-1 Goldade SBAC Estimated Costs 85
Table 7-1: Heat loss of Goldade House 93
Table 7-2: Meteorological Data For Reno, NV Latitude 39.5^o 95
Table 7-3: Monthly Heating Load for Goldade House (L ~ Joules) 96
Table 7-4: Determination of H_T, the Total Average Daily Radiation Incident on the Collector 100
Table 7-5: Calculations to Determine F and Qs 101
Table 7-6: Economic Comparison of Five Backup Heating Fuels in Northern Nevada 103

List of Figures

Figure 1-1: Roof Example Figure 1-2: Roof Example Figure 1-3: Side Wall Example 7
Figure 1-4: DRI Solar Research Laboratory with SBAC Roof 10
Figure 3-1: MSEL Sketch 21
Figure 3-2: Generic Collector Efficiency versus Flow Function Curve 22
Figure 3-3: Fiberglass glazing transmissivity τ versus incidence angle θ. 24
Figure 4-1: MSEL 41
Figure 4-2: MSEL and Collector 41
Figure 4-3: Solid Works 3'' Throat Nozzle Design with Taps 46
Figure 4-4: Tap Pressure Design 47
Figure 4-5: Transformer Piece 47
Figure 4-6: Completed Nozzle Design 44
4-7: Duct Configuration 48
Figure 4-8: Commercial Air Flow Meter 50
Figure 5-1: Geometry and heat transfer coefficients for the Goldade Collector 58
Figure 5-2: Theoretical Performance Curve for the Goldade Collector. 73
Figure 5-3: $T_{in} = T_{amb}$ 74
Figure 5-4: $T_{in} = T_{out}$ 75
Figure 5-5: Intermediate Point 75
Figure 5-6: Field vs Theoretical Curves of Goldade House 77
Figure 6-1 Goldade SBAC 80
Figure 6-2 Front View of Goldade SBAC Sketch up 81
Figure 6-3: Side View Cut Away of Goldade SBAC 82
Figure 6-4: SBAC and House 83
Figure 6-5: Duct Configuration 84
Figure 6-6: RS10 Blower Curve 84

Nomenclature

A_c	Aperture area of the collector
A_D	Area of duct
A_T	Area of nozzle throat
A_1	Area of nozzle straight
ACH	Air Changes Per hour
Alt_{KM}	Altitude at a location in Kilometers
C_D	Nozzle discharge coefficient
Cp	Specific heat of air
d	distance between surface i and j in the collector
DD	Degree Days
D_H	Hydraulic Diameter
f	Friction factor or fraction of heating load supplied by collector
F'	Efficiency Factor
F_R	Heat Removal Factor
g	Gravitational Constant
G_{sc}	Solar constant
H	Height of collector, or total average daily horizontal radiation
H_b	Monthly daily average horizontal beam radiation
H_d	Monthly daily average horizontal diffuse radiation
H_T	Monthly daily average radiation striking collector
H_O	Monthly daily average outer space radiation at specified latitude
h	General radiative or convection coefficient
h_c	General convection heat transfer coefficient
$h_{c,c-a}$	Convection heat transfer coefficient between the cover and the ambient
$h_{c,i-j}$	Convection heat transfer coefficient between the previous and next layer
$h_{c,p-c}$	Convection heat transfer coefficient between the plate and the cover
$h_{r,g-a}$	Radiation heat transfer coefficient between the cover and the ambient
$h_{r,i-j}$	Radiation heat transfer coefficient between the previous and next layer
$h_{r,p-c}$	Radiation heat transfer coefficient between the plate and the cover
h_w	wind heat transfer coefficient
I_b	Horizontal beam radiation
I_{bT}	Hourly beam radiation on a tilted surface
I_d	Horizontal diffuse radiation
I_{calc}	Insolation calculated striking surface of collector at specified time
I_{dT}	Hourly diffuse radiation on a tilted surface
I_o	Hourly extraterrestrial radiation at a set longitude and time
I_{on}	extraterrestrial normal Irradiance
I_{RT}	Hourly reflected radiation on a tilted surface
I_T	Total hourly radiation striking a tilted surface,
I_{Ti}	Total instantaneous radiation striking a tilted surface,
K_{air}	Thermal conductivity of air
K_{ins}	Thermal conductivity of insulation

K_M Constant for Venturi nozzle or velocity meter
K_{pw} Thermal conductivity of plywood
K_T Clearness index for an area
k_n Thermal conductivity of material "n"
L monthly total heating load for space heating
L_{ins} Length of insulation in inches
L_n Length of material "n"
L_{pw} Length of plywood
m mass flow rate of air
n Day of the year (1 to 365)
N Number of collector covers, or number of days in a month
Nu Nusselt Number
P Flow function $(T_{in}-T_{out})/I$
P_1 Pressure in the Venturi nozzle entrance
P_a Ambient pressure
P_V Pressure difference in Venturi nozzle
P_T Pressure in Venturi nozzle throat
Pr Prandtl Number
Q_{inf} Heat loss (or gain) of house due to infiltration
Q_{loss} Total heat loss of the collector
Qu Total heat produced by collector
R Universal gas constant or generalized thermal resistance network
R_b Ratio of beam radiation on a tilted plane to that on the horizontal; or total resistance network of the back of the collector
R_{c-a} Heat resistance network between the cover and ambient
Re Reynolds Number
R_{conv} Heat resistance network for convection heat transfer
R_{p-b} Heat resistance network between the plate and the back
R_{p-c} Heat resistance network between the plate and the cover
R_{rad} Heat resistance network for convection heat transfer
R_T Heat resistance network between the plate and the ambient or the top of the collector
$T_{,avg}$ Average fluid (air) temperature in thermo-resistance network
$T_{a,avg}$ Monthly average temperature
T_{amb} Temperature of ambient
$T_{f,e}$ Temperature of the fluid exiting the collector
$T_{f,i}$ Temperature of the fluid entering the collector
T_i Temperature of previous layer
T_j Temperature of current layer
T_p Temperature of the absorber plate
T_{ref} Reference temperature (100 ^oC)
U_B Total heat loss coefficient of the bottom of the collector
U_L Overall total heat loss coefficient
U_T Total heat loss coefficient of the top of the collector
V General Velocity term.

V_T Velocity of the nozzle throat
V_1 Velocity of nozzle straight
V_{wind} Velocity of the wind
V_{SI} Wind speed in mph
X Dimensionless unit to determine f-Chart
Y Dimensionless unit to determine f-Chart

Greek

α Absorptivity of the absorbing plate
β Tilt angle of the collector from horizontal, nozzle duct expiation coefficient, coefficient of volume expansion
γ Angle of the collector from due south
δ Declination, or characteristic length
Δ Change in unit
ΔP_V Change in pressure over nozzle throat
Δt Total number of seconds in a month
ΔT total temperature change from inlet to outlet of the collector
ε_b Emissivity of the back of the collector
ε_c Emissivity of the glazing cover
ε_p Emissivity of the plate
η Efficiency
$\eta_{y\text{-}int}$ Y-intercept efficiency for steady state curve
θ Angle between surface normal and incident radiation
θ_z Zenith Angle
ρ Reflectance; density
σ Stefan Boltzmann Constant
τ Transmittance
τ_{act} Actual transmittance for non-normal oriented collector
$\tau\alpha_{avg}$ Monthly Absorption and Transmittance Product
υ Kinematic viscosity
φ Latitude of the collector in radians
ω Hour angle
$\Sigma \frac{L_n}{k_n}$ Summation of the lengths of materials divided by their thermal conductivity

Introduction

The American Great Basin – Southwest Region features abundant year round sunshine with cold winters. Since energy has been historically cheap, buildings and water are heated via fossil-fuel derived sources, and the vast solar heating potential is largely untapped. As populations increase, this permanent demand on limited fossil fuel is non-sustainable, so a sustainable approach must be developed. Also, concern has been expressed regarding CO_2 emissions to the atmosphere resulting from hydrocarbon burning (Clean Energy Authority, 2015), (U.S. Energy Information Administration, 2004), (U.S. Energy Information Administration, 2015).

Solar space and water heating systems have not achieved their potentials due to high initial costs. To partially assuage excessive expense, some government and utility entities offer pecuniary incentives to homeowners and businesses to promote solar usage. Generally, such inducements are extended to systems whose collectors have been certified by the Solar Rating and Certification Corporation (SRCC) (NV Energy, 2015). The SRCC is a non-profit organization whose purpose is development and implementation of national rating standards and certification programs for solar energy equipment. The SRCC provides independent third-party certification for solar collectors and is wholly funded through fees paid by companies disseminating solar equipment. The SRCC is the recognized certification authority in the United States for rating and ranking commercially produced solar collectors.

It is reasonable that entities providing financial incentives to promote solar implementation would want to assure their money is applied toward proficient solar collectors competently installed. Therefore, nearly all solar collectors sold and installed in the United States have been rated by the SRCC, and the consumer can assure the incentive sponsor that substandard equipment is not being installed (Solar Rating & Certification Corporation, 2015).

Factory fabricated solar hardware is inherently expensive to the consumer because so many people make a living from each sale, in addition to shipping (and often importation) costs. However, there is an alternative to expensive factory-manufactured solar systems, namely site-built air-heating solar collector systems. Such solar air heating systems are built onto a building as a part of the structure, from basic materials. Chapter 1 discusses these systems.

Although site-built air-collectors (SBAC) are much less expensive than commercial systems, they have not been widely promoted because there is little money to be made by such advertisement. Furthermore, laymen do not know the basics of how to build such a system and specify obligatory components, such as the blower and thermostat. Although plans for site-built systems can be specified, there is another impediment to implementation of site-built systems, namely they are not SRCC evaluated and therefore generally not subject to financial incentives by government and utilities (Nevada State Legislator, 2015), (NV Energy, 2015), (South West Gas, 2015). Since financial incentives promote adoption of any article, site built systems are at an

inherent economic disadvantage relative to commercial systems because they are not SRCC rated.

This thesis is bifurcated into two parts. Part 1 examines air heating solar collectors on both a theoretical and empirical basis. The construction of a Mobile Solar Evaluation Laboratory (MSEL) is described, built and demonstrated. The MSEL is intended to facilitate field evaluation of SBACs, and adhere to SRCC Standards as closely as possible. When field-testing proves that a site-built collector has an efficiency that meets a set standard, then incentive grantors can support these systems with as much confidence as commercial systems, promoting their adoption. The MSEL is tested on the Goldade site-built air collector in the Minden, Nevada area as demonstration, and efficiency curves are propounded for the unit from both experimental and theoretical methodologies.

The research involves how SRCC certifies modular air collectors, what equipment is used, required conditions, and procedures utilized to test conventional air collectors. The MSEL is developed to practically replicate SRCC procedures and methodology to accurately develop efficiency curves for SBACs in the field. An error analysis accompanies the algorithm.

Part 2 consists of the technical and economic assessment of the Goldade Solar Heating System in Minden, Nevada. In anticipation of this thesis, Family Goldade built a 128 ft^2 (11.9 m^2) solar collector to provide winter space heating for the Goldade Home. The system construction is documented and system cost estimated two ways: 1) actual

cost (since Goldade labor was free) and 2) materials and estimated labor cost. MSEL estimates collector efficiency under different conditions. The total heat contribution for a winter, using historical winter weather data, are estimated on a month-by-month basis using the f-chart method. The solar system payback period is thus estimated. Calculations indicate that SBACs reduce appreciable CO_2 emissions to the atmosphere.

Chapter 1. Site Built Air Collectors (SBAC)

Solar heating systems have been employed for over a century (Perlin, 2015). The first commercial solar water heater was patented in 1891 (Perlin, 2015). Within 5 years, about 30% of homes in Pasadena, California had installed solar domestic hot water systems (Pahl, 2003). Although the solar hot water heating industry had spread to Florida by the 1930s, copper shortages during World War II (coupled with economic incentives offered by electric companies to switch to their hot water heaters) crippled the burgeoning solar hot water industry (Pahl, 2003). The advent of massive natural gas discoveries and inexpensive energy attenuated interest in solar heating.

Water heating is the largest natural gas end use in California, consuming 38% of residential and commercial gas (Perlin, 2015). Sixty-five percent of the energy used to heat water in California can be saved with solar water heating (SWH) (Perlin, 2015). From 1975 through 1985 California installed approximately 159,000 SWH systems, motivated by utility incentives and tax credits (Mowris, 2010). During the Solar Decade (1975-84) federal tax credits (40% of solar system cost) and state tax credits (55% in California) stimulated widespread installation of solar DHW (domestic hot water) and space heating systems, but after the tax credits were discontinued the market evaporated (Turner, 2015). Many liquid-based systems failed due to leaks or freeze damage (Turner, 2015). The economic non-viability of commercial solar systems absent

government or utility incentives persists to this day, which is why they are rare even in sun-blessed areas.

Collectors drive the cost for most solar heating systems. Commercially produced solar collectors are quite expensive, and in side-by-side studies SBACs have been shown to be much less pricy (Hoekman, Broch, Robbins, Jacobson, & Turner, 2012).

SBAC systems can be built into a building much less expensively than equivalent commercial solar heating systems, both retrofit and new construction. Site-built solar hot air systems are: 1) simple; 2) robust; 3) easy to maintain; 4) have no liquid to leak, freeze, overpressure (boil), corrode, or degrade; 5) very flexible; (6) capable of being built by homeowners with modest skills; (7) somewhat indifferent to leakage; and 8) cost 1/3 relative to commercially installed solar collectors (Hoekman et al., 2012), (Beard, 1993).

SBAC systems have been built and used for many years in the Reno area. Figure 1-1 shows a residential 600 ft^2 solar air-heating collector built into a new construction residential roof in 1991 in the Sierra Nevada Mountains near Reno, Nevada at elevation 6000 feet. A detailed study suggested the simple payback period (SPP) would be 3 years, and 12 years living in the house validated the 3 year SPP (Kiley, 1992), (Turner, 2015).

Figure 1-2 shows a 208 ft^2 solar air heater retrofitted to a house roof in Bend, Oregon in 2005. This unit was built from basic materials by the homeowner and

provided year round DHW and winter space heating. The system was economically attractive (Turner, 2015).

Workmen with modest skills can retrofit a solar space heater on the south wall of a house. The unit in Figure 1-3 heats a house in Reno, Nevada and demonstrated a 3 year simple payback period without external incentives (Turner, 2015).

Figure 1-1: Roof Example

Figure 1-2: Roof Example

Figure 1-3: Side Wall Example

There are many advantages to site-built solar air heaters. The house itself can act as the collector support, in this case the house insulation is also the collector insulation. The collector is the building exterior finish (roof or south wall) and even irregular geometry blends into the architecture of the building (Figure 1-3). There is no liquid to leak, freeze, overpressure (boil), corrode, or degrade. The approach is widely applicable for new construction or retrofit, and is easy for architects, builders, homeowners and others to comprehend and implement. Its manufacturer guarantees the external glazing for 20 years, validated by the house in Figure 1-1 (Turner, 2015). The list of materials consists of: fiberglass glazing; thin black metal sheets; 2 x 4 wood

studs; 1½ inch wide aluminum strips; various screws and bolts; caulk; rubber stripping; a blower; thermostat; and ducting. If DHW heating is intended, then an air-to-water heat exchanger and solar hot water storage tank are also specified, as was done in the Figure 1-1 and Figure 1-2 houses. All materials are widely available and most are fabricated domestically. Beginning level contractors and many homeowners possesses the requisite skills. Money paid for labor stays in the local community. The system is robust and maintenance requirements are minimal (Temple & Adams, 1980), (Turner, 2015).

The 230 ft^2 homeowner-built retrofit application shown in Figure 1-3 cost $1200 to build (including $300 for a labor assistant) and saves about $400/year in propane heating costs. The simple payback period is 3 years, and if government or utility financial incentives had been available the payback period would be less. If a 230 ft^2 commercial system had been installed, the cost would have been approximately $10,000, and even with incentives the homeowner would not have bought it (Turner, 2015).

Advantages claimed for a site-built air heating solar collector over hydronic (liquid filled) collectors include: 1) Cost; 2) Small leaks are unimportant; 3) Hydronic systems can over-pressure in summer, and anti-freeze degrades with time; 4) Freeze and corrosion problems are eliminated; 5) Part of the expense is defrayed by not having to install a conventional roof or wall finish, and the collector insulation is often coincident with the house insulation; 6) The solar system can blend into the building

architecture (Figures 1-1 and 1-3); 7) economic efficiency higher; 8) can be built by skilled laymen; and 9) money for construction stays in the local community, instead of supporting foreign economies.

However, there are many reasons that site-built solar air heaters have not been implemented. Some of the market impediments include:

1. Public perception that solar collectors are only available commercially in factory standard sizes, and are hydronic. This is because solar contractors promote what can make them money, and site-built systems obviate such middleman companies.
2. Ignorance how to properly prospect a site, size and design a solar system, obtain a building permit, and build it without mistakes. Authoritative guidance is needed.
3. Uncertainty about the technical and economic performance of site-built solar systems.
4. Difficulty obtaining building permits for non-commercial solar systems.
5. Lending institutions are unfamiliar with the site-built solar approach.
6. Non-commercial systems typically do not qualify for most economic incentives. In Nevada such financial inducements are limited to SRCC-rated systems, which excludes site-built systems.

In 2011 the Desert Research Institute in Reno, Nevada, constructed a 578 ft^2 (53.8 m^2) SBAC that is the south facing roof of a Solar Research Laboratory, shown in Figure 1-4. The collector is driven by a variable speed air blower that can vary between 1000 cfm to 1800 cfm. The heated air passes through air-to-water heat exchangers, and during summer 2012 trials the system heated 240 gallons of water to over 160^oF at no load (Hoekman et al., 2012).

Figure 1-4: DRI Solar Research Laboratory with SBAC Roof

SBACs have been built in different parts of the United States. An excellent 1980 book provides detailed architectural plans for both roof and wall mounted SBACs in new construction houses as well as retrofits (Temple & Adams, 1980).

Previous Work

The concept of a site built air collector (SBAC) has been around for a while, but has never been highly developed, widely understood, advertised, nor generally accepted. Building departments are generally adverse to SBAC systems, even when system plans have been engineered and stamped, because most plan-check engineers do not understand them and there is nothing in the Uniform Building Code (UBC) regarding solar heating.

This lack of attention arises from the inherent non-commerciality of SBACs. Since they are often built on a house as part of a house, constituting a "functional working exterior surface" of a building built from basic materials by homeowners or local craftsmen, companies cannot mass-produce them. Therefore there has been neither advertisement nor professional advocacy groups for SBACs. When most people contemplate solar space or water heating, they think of modular collectors, generally hydronic units.

This situation indicates the need for a reeducation program, to familiarize consumers in appropriate locations with the idea of SBACs as practical solar heaters. But the technology diffusion will require either word-or-mouth or government programs, or licensed builders locally advertising their capabilities and building solar heaters to approved specification.

Since very little work or interest has been committed to SBAC systems, it is not surprising that SBAC technology lags behind other technologies, because very few systems have been built and demonstrated.

A 1980 book discusses SBACs in considerable detail (Temple and Adams, 1980). However, the book is rife with intricate detail and not very readable for the layman.

In the early 1980s Dr. Turner (Turner, 2015) commercially designed the solar component of about 20 upscale solar houses for private clients, working with architects and homeowners. At this time the State of California offered a 55% solar tax credit, and the federal government offered a 40% solar tax credit. In some cases both tax credits could be summed, so the total tax credit could be 95%. This promoted vigorous solar adoption, but mixed in with technical and economically efficient designs were junk systems that often led to lawsuits. In 1983 both the federal and California governments announced that the tax credits would terminate in 1985, which abruptly ended the Solar Decade. In the past 30 years there has been precious rare interest or SBAC reporting in the literature.

The most recent study found pertaining to SBAC economics was a study conducted by Deakin University in 2007 on a SBAC constructed on their campus. They found that this particular collector was improperly installed, and not suitable for winter time heating. As the collector's orientation was horizontal, and there were faulty controls at the time of study. It is unlikely this particular SBAC was actually contributing to the heating load because of these issues. They concluded, that if the collector were

properly orientated and installed, it could potentially offset around 50% of the winter time space heating load (Rogers, Fuller, & Luther, 2007).

Perhaps the most relevant study found was a thesis at the University of Nevada Reno (UNR) conducted by Matthew Kiley in the early 90's. This thesis evaluated the technical and economic performance of a SBAC installed as part of the roof structure of Dr. Turner's house (Figure 1-1). The SBAC was utilized for winter space heating and year-round domestic water heating. This study found a payback period of 2.5 to 5.5 years for the collector system depending on the usage (Kiley, 1992).

A few studies were found that compare the technical-economic performance of differing air collector configurations with the goal of determining the air collector configuration that will provide the highest ratio of thermal performance to estimated collector cost. Another thesis from UNR by Joe Beard evaluated the economic performance of several air collector configurations. This study concluded that air collectors consisting of low cost slotted screens for an absorber and a glazing cover to be the best technical-economic performers (Beard, 1993). A similar study concluded by Donatien Njomo at the University of Yaounde in Cameroon compared the technical and economic performance of air collectors consisting of glass and glazing covers. This study concluded that air collectors consisting of glass covers thermally out preformed their glazing counter parts. However, glazing covers were more economical (Njomo, 1994).

Chapter 2. Incentives & SRCC Standards for Solar Air Heaters

An internet search will discover many sites and sources for site-built solar heating, many of which include instructions with amateur errors (Pahl, 2003), (Mother Earth News, 2015), (EVsRoll, Undated). This is why incentive grantors in Nevada are rightly suspicious of SBACs; they don't want to incentivize deficient collectors. Due to these concerns, incentives awarded by Nevada (and generally American) agencies for solar installations are almost exclusively certified by the SRCC (Nevada State Legislator, 2015), (NV Energy, 2015), (South West Gas, 2015).

The SRCC (Solar Rating and Certification Corporation) is a non-profit institution based in Florida, with testing laboratories across the US which rate all unitized collector types and designs. The customer pays the testing fees. Thus, a company that wants to sell collectors sends a model to the SRCC, which tests the collector, generates performance curves, and certifies the model performance. Then when the company sells that model it has been SRCC-certified, and an incentive sponsoring entity can have confidence that the system will perform to a known high standard. Due to the nature of the testing conducted by the SRCC, all SRCC-certified solar systems are modular. If the incentive grantor requires SRCC rating, then no incentives are awarded to custom installations, despite the many advantages outlined in Chapter 1.

A list of Nevada incentives for renewable energy systems and installations is available online, and are most often in the form of monitory rebates, low interest loans

or tax exemptions (NV Energy, 2015), (Clean Energy Authority, 2015), (South West Gas, 2015), (U.S Department of Energy, 2015). There are incentives available for most renewable energy projects, including solar air collector systems. There are a total of 12 applicable programs according to the Nevada Data Base of State Incentives for Renewables and Efficiency (DSIRE) (U.S Department of Energy, 2015). This list is as follows:

1. Nevada Renewable Energy Systems Property Tax Exemption: is a state run tax exemption to encourage all forms of renewable energy in the state, including Solar Space Heating. The system installed will be exempt from property taxes provided it is a qualified system by the state of Nevada (Nevada State Legislator, 2015). This currently means the collectors will be SRCC-certified.
2. Tribal Energy Program Grant: this is a Department of Energy (DOE) program intended to promote "energy sufficiency, economic growth, and employment on tribal lands through the development of renewable energy and energy efficiency technologies" through financial incentives. This is a competitive application process, in which a tribe recognized by the government will apply for energy efficiency grants (U.S. Department of Energy, 2013).
3. Energy Efficient Mortgages is a federal program that credits a home's energy efficiency in the home loan. The loan amount is limited by the projected savings of the home, via energy upgrades (U.S. Department of Energy, 2013).

4. Business Energy Investment Tax Credit (ITC): Is a Corporate Tax Credit in which up to 30% of the cost of the installation of a solar system will be deducted from the taxation by IRS from the business taxes of that fiscal year of installation (NV Energy, 2015).
5. NV Energy Solar Generations Solar Heating: This is a rebate program awarded by the utility company for all SRCC-certified solar thermal systems. This program is structured differently for the differing customers. For residential customers the maximum rebate is 30% of the cost of the system up to $2,250. For small business, non-profits, and government customers the grant amount is awarded based on the thermal performance of the system. Small Businesses are capped at $7,500; non-profits and government entities are capped at $30,000 of grants (U.S Department of Energy, 2015).
6. Green Power Purchasing Goal for Federal Government: Is a regulatory program for all new federal buildings in which a specified percentage of the energy consumed by the building must be supplied by some form of renewable energy. Currently the regulation requires that federal buildings must have 7.5% of their energy supplied by renewables. This percentage will incrementally rise until 2025 when 30% of energy consumed must be supplied by renewables (U.S Department of Energy, 2015).
7. Energy Portfolio Standard: Is a state standard passed in 1997. Under this standard NV Energy must use eligible renewable energy resources to supply a minimum of 25% by 2025. All forms of renewable energy or energy efficiency are eligible;

however under this standard a minimum of 5% of the total energy supplied must be via solar energy systems (U.S Department of Energy, 2015).

8. Nevada State Energy Reduction Plan: Is a state regulatory policy, in which all state owned buildings are required to have a minimum of 20% of their energy be supplied by renewables (U.S Department of Energy, 2015).
9. USDA Rural Energy for America Program (REAP) Grants: Is a competitive grant or loan program for all rural small businesses. This provides financial assistance to agricultural producers and small businesses in rural America to purchase, install, and construct renewable energy systems. The grants are limited to 25% of the systems cost and loans may not exceed $25 million (U.S Department of Energy, 2015)
10. Modified Accelerated Cost-Recovery System (MACRS): Is a federal financial incentive in which corporations may list any form of renewable energy as a 5-year depreciation on their tax returns (U.S Department of Energy, 2015).
11. Property-Assessed Clean Energy (PACE) Financing: is a state financial incentive in which property owners borrow money to fund energy improvements. The loan is typically repaid via a “special assessment” on the property over a period of years (U.S Department of Energy, 2015).
12. Renewable Energy Systems Property Tax Exemption: As its name entails, this is a tax exemption for all commercial, industrial or agricultural businesses for all renewable energy systems (U.S Department of Energy, 2015)

It is clear that SRCC rating for collectors is a prerequisite for gaining incentive support for solar heating systems in Nevada and elsewhere. Naturally, a site-constructed solar air heater cannot be inspected by SRCC, although arguably SRCC could examine a generic plan and certify a system built exactly to the plan. But this is not what SRCC does. And a site-built system erected by amateurs might not exactly adhere to a prescribed plan.

Currently, site-built solar heating systems are built by only a small environmentally conscious community, but, these cost effective systems could potentially become common place if government and utility encouragement were available, and building departments were informed and educated. The above discussion has defined a need in Nevada and elsewhere for field certification of SBACs, so incentive sponsors can confidently encourage them. Such field testing must be inexpensive but scientifically reliable. This thesis responds to that need by developing a Mobile Solar Evaluation Laboratory (MSEL) that approximates the exacting ASHRAE 93-2010 Standard to which SRCC adheres, but can be quickly performed in the field by a trained technician.

Chapter 3. Replicating SRCC Standards in the Field for Site Built Air Collectors

A primary objective of this thesis is to create and demonstrate a Mobile Solar Evaluation Laboratory (MSEL) to generate a SBAC efficiency curve quickly, accurately, and inexpensively. This by definition would be a modular unit, which would be designed to portably field test any collector in a single visit over a period of a few hours, when the weather and season were conducive to solar testing. This differs from SRCC solar ratings as their rating process is rigorous, detailed, and time consuming. It is not uncommon for a SRCC rating of a solar thermal collector to take over 6 weeks because of the stringent standards by which they abide. SRCC waits for a 'perfect solar day' to run their tests. The test collector is mounted so the collector surface is normal to the sun rays, which is not possible with a SBAC. The procedure is quite expensive typically starting at $1,000 and ranging to over $10,000 depending on the system. Furthermore, the client company has annual fees, to renew their licenses for each year the collector is in production (Solar Rating & Certification Corporation, 2015).

SRCC certification inherently makes evaluations of SBACs impractical, and the cost would be unfeasible. Furthermore, SRCC is able to test solar collectors any time of the year by orienting the units on a stand so they face in any direction. A SBAC is generally built into a building and cannot be moved; as such, it is not possible to test a south facing vertical wall system in summer. Currently, any governmental or private incentives for thermal collectors must be rated by the SRCC first. This makes any SBAC

infeasible to incentivize and less attractive to home owners and contractors alike, despite the fact that, the cost/ft^2 for SBACs is typically a fraction of that of their modular counterparts, and they manifest comparable performance (Temple & Adams, 1980), (Beard, 1993).

Therefore, to stimulate deployment of cost-effective site-built solar systems, which save owners money and reduce fossil fuel consumption with attendant CO_2 emissions reduction, an effective but inexpensive capability must be developed to discriminate between proficient and sub-par site-constructed systems. Such an available expertise would allow incentive grantors to confidently grant incentives to qualified SBACs.

This chapter defines what parameters must be measured to replicate an SRCC efficiency curve for a stationary collector. An error analysis quantifies the impact that uncertainty in each measurement will manifest in the efficiency estimate, and allows limits on the assessment. Chapter 4 describes construction the MSEL on a component-by-component basis.

As is shown in Figure 3-1, air will be blown in to the collector in a closed or open system depending on if the butterfly valve is opened or not. Temperature and pressure will be measured by Pressure Transducers (PT) and Thermocouples (TC) in the various locations. These values along with the incident radiation striking the collector and the ament pressure allow for sufficient data to determine the efficiency of the collector under given conditions. The MSEL has the requisite sensors and equipment to measure

all these data. Chapter 4 goes into greater detail of how the MSEL is operated and its equipment is setup.

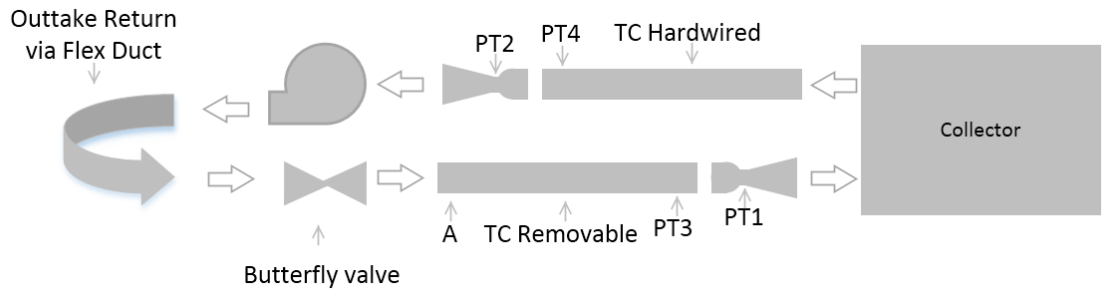

Figure 3-1: MSEL Sketch

The curve of collector efficiency versus flow function indicates which parameters need to be measured. Figure 3-2 shows a generic efficiency versus flow function curve e.g. (Duffie & Beckman, 1980).

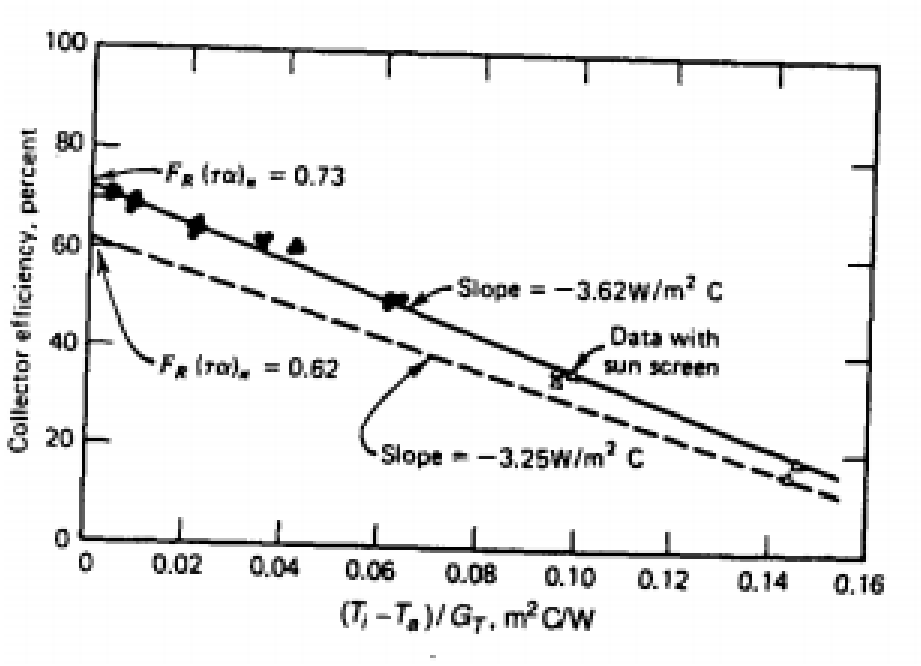

Figure 3-2: Generic Collector Efficiency versus Flow Function Curve (Duffie & Beckman, 1980)

The efficiency η on the ordinate (y-axis) is given by:

$$\eta = \frac{Useful\ Heat\ Out}{Solar\ Heat\ Recived} = \frac{\rho Q C_p (T_{out} - T_{in})}{I A_c}$$ Equation 3-1

Where:

ρ = Density of the air at the measurement of flow (kg/m^3)

Q = Volumetric Flow rate (m^3/s)

I = Insolation striking the collectors surface (W/m^2)

A_c = Area of the collector (m^2)

T_{in} and T_{out} = Temperature entering and exiting the collector respectively (°C)

Cp = Specific heat of air (1005 J/kg-^{o}C)

The flow function on the abscissa (x-axis) is

$$P = \frac{T_{in} - T_{amb}}{I} \qquad P \approx m^2\text{-}°C/W \qquad \text{Equation 3-2}$$

The air volumetric flow rate Q is measured using a flow meter or more standardly a Venturi nozzle. If for small flows and diameters a flow meter is employed, it will previously have been calibrated with a Venturi tube.

There is another parameter which must be measured, namely the angle between the collector surface normal and the sun, θ. The transmissivity of the glazing (τ), which is defined as the ratio of radiation passing though the glazing to that striking the glazing. Insolation striking the absorber will diminish as the angle of incidence θ increases. Figure 3-3 shows τ versus θ for the fiberglass glazing material that is utilized on all collectors in this study (Solar Components Corporation, 2015).

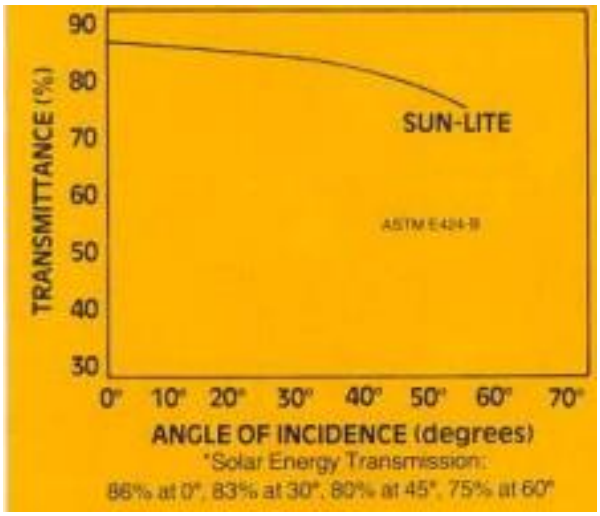

Figure 3-3: Fiberglass glazing transmissivity τ versus incidence angle θ (Solar Components Corporation, 2015).

Figure 3-3 indicates specific values for clean glazing: τ =0.86 at $\theta = 0^o$, 0.83 at 30^o, 0.80 at 45^o, and 0.75 at 60^o. Therefore, if measurements indicated a given efficiency $\eta_{60}{}^o$ when $\theta = 60^o$, the efficiency for a clean single glazing unit could be normalized to $\eta_0{}^o = \eta_{60}{}^o (0.86/0.75)$, or about 14.7% higher. If a double-glazed unit were examined the factor would be $(0.86/0.75)^2$, or about 31.5% higher.

The 8 parameters that must be measured are:

1. ΔP_V : $= P_1 - P_T$ in the Venturi section, needed for Q (kPa)
2. T_{Amb}: Ambient air temperature (°C)
3. T_{out}: Collector air exit temperature (°C)
4. T_{in}: Collector air inlet temperature (°C)
5. P_A : Atmospheric pressure (kPa)
6. I: Insolation striking the collector surface (W/m^2)

7. A_c: Solar collector face area (m^2)
8. θ: Angle of incidence between solar rays and collector face normal.

Additionally the wind velocity V_{wind} should be noted for each measurement, although V_{wind} does not appear in the calculations. SRCC does not record measurements when V_{wind} is too large (greater than 5 mph), because it diminishes the collector top loss coefficient and reduces the apparent efficiency relative to a windless or low wind day (Solar Rating & Certifiaction Corporation, 2014).

If a velocity meter is used to measure volumetric air flow rate instead of a Venturi meter, then in Equation 3-1 $Q = A_D * V$, where A_D is the area of the duct the velocity was measured. So, instead of measuring ΔP_V it is necessary to directly measure V. Then in the 8-numbered list above V replaces ΔP_V. Although both measurement methods can yield reliable results, the hand-held velocity meter is more simplistic, quicker to make measurements, and less expensive to use than the Venturi meter. However, as demonstrated below, a measurement error in V gives a linear error in calculated efficiency, whereas an error in measuring ΔP_V manifests only in the square root in the efficiency calculation.

Having defined 8 parameters which must be measured to construct an efficiency versus flow parameter curve, it is necessary to develop a sensitivity analysis to estimate how the impact of a measurement error will manifest on the calculated efficiency. This error analysis will be conducted for each measured parameter.

Error analysis techniques are well developed and will be briefly summarized here. Suppose a set of measurements is taken and the uncertainty in each measurement is estimated to be x_i, x may be a ± variation specified by the manufacturer of a monitoring device, or may be estimated from a large number of measurements, where members of a main sequence deviate from a regressed best-fit curve (Holman, 1984). It is necessary to estimate the uncertainty in a calculated result (here η) based on the uncertainties in the primary measurements. The result η is a function of the independent variables, or $\eta = \eta(\Delta P_v, T_{amb}, T_{out}, T_{in}, P_A, I, A_c, \theta)$ (for a Venturi section measurement)

If velocity is directly measured, then ΔP_v is replaced by V for the efficiency parameter. Then the uncertainty (error probability) is related to the partial derivatives of η with respect to each parameter (Holman, 1984). Then:

$$x_\eta = [\,(\frac{\partial \eta}{\partial \Delta P_V}\, x_{\Delta P_V})^2 + (\frac{\partial \eta}{\partial T_{amb}}\, x_{T_{amb}})^2 + all\ other\ terms\,]^{½} \qquad \text{Equation 3-3}$$

Air volumetric flow rate (Q) through the collector is the most difficult parameter to quantify, and uncertainties in flow rate accuracy can lead to the greatest error in the efficiency. There are two common ways to estimate flow rate; 1) using a Venturi Meter, which converts a measured pressure drop to velocity and hence to flow rate, and 2) employing a hand held velocity meter which directly measures velocity.

SRCC uses a Venturi Nozzle because it is the standard, easy to install in a controlled test environment, and cost is not a factor. The Venturi Nozzle is the most accurate flow rate measurement device, and the pressure difference between the straight pre-section and the nozzle throat can be accurately measured and the results immediately transcribed to a computer. ASHRAE has defined a standard for Venturi Nozzles in (ASHRAE Standard 41.2-1987, 1993), and SRCC has adopted these recommendations for their specific uses (SRCC Standard 100-2014-07, 2014).

Bernoulli's equation and conservation of mass govern behavior of the Venturi tube, providing a mathematical description of how pressure decreases with increasing velocity (Cengel & Turner, 2001). Accordingly, with subscript "T" designating 'Throat" of the nozzle and subscript "1" a larger straight section leading to the nozzle throat (See Figures 4-3 to Figure 4-6 in the next chapter):

$$P_1 + \frac{1}{2}\rho V_1^2 = P_T + \frac{1}{2}\rho V_T^2 \qquad \text{Equation 3-4}$$

$$Q = A_1V_1 = A_TV_T \qquad \text{Equation 3-5}$$

Eliminating velocities from the above three equations yields,

$$Q = A_T \sqrt{\frac{2(P_1 - P_T)}{\rho\,[1-(\frac{A_T}{A_1})^2]}} \qquad \text{Equation 3-6}$$

Where:

P_1 and P_T = Pressure in the duct and nozzle throat respectively (kPa)

V_1 and V_T = Velocity in the duct and nozzle throat respectively (m/s)

A_1 and A_T = Area in the duct and nozzle throat respectively (m^2)

Since A_1 and A_T can be measured precisely, the parameter in which care must be taken during measurement is: $\underline{\Delta P_v = P_1 - P_T}$.

The air density ρ must be measured at the point where Q is measured. Then the Perfect Gas Law, $\rho = P_A/RT$, which is exact for atmospheric temperature (T) and pressures (P_A) must be utilized (Cengel & Turner, 2001).

Equation 3-1 combined with Equation 3-6 and $\Delta P_v = P_1 - P_T$ yield the efficiency in terms of measured parameters when flow is measured via a Venturi meter. Thus, assuming flow measurements are taken at the collector outlet [high temperature (T_{out})], Equation 3-7 is developed. If the flow measurement is taken at the collector inlet, then the $(T_{out})^{½}$ is replaced with $(T_{in})^{½}$ in the denominator.

$$\eta = \frac{K_M \sqrt{P_A \; P_V}\,(T_{out} - T_{in})}{I\sqrt{T_{out}}} \quad where\ K_M = \frac{\sqrt{2} C_D \; A_T \; c_p}{A_c \sqrt{1-(\frac{A_T}{A_1})^2}\sqrt{R_{air}}} \qquad \text{Equation 3-7}$$

Where:

C_D = Nozzle discharge coefficient (Dimensionless ~ C_D = 0.98 used in this report)

P_A = Pressure ambient (kPa)

P_V = Pressure difference in nozzle and duct (kPa)

R_{air} = Universal gas constant of air (0.287 kPa-m^3/kg-^oK)

C_D is a Venturi nozzle discharge coefficient, typically in the range of 0.98 when the Reynolds Number is above 2 x 10^5 (ASHRAE Standard 41.2-1987, 1993). For the majority of the tests Re was 5 to 6 x 10^5, so, C_D = 0.98 will be used in this study.

In Equation 3-7 all parameters in K_M are simple to accurately measure, or are predetermined values, as such K_M is considered a constant. Equation 3-7 is the starting point for a sensitivity analysis when using a Venturi nozzle. Since Bernoulli's Equation (Equation 3-4) has pressure and density to the first power and velocity to the second power, the density (and therefore P_A and T_{out}) and ΔP_V appear in Equation 3-7 to the square root power.

Taking the partial derivative of η (Equation 3-7) with respect to ΔP_V yields the first term on the right hand side of Equation 3-3. Then:

$$\frac{\partial \eta}{\partial \Delta P_V} = \frac{K_M \sqrt{P_A}\,(T_{out} - T_{in})}{2I \sqrt{P_V}\,\sqrt{T_{out\ or\ in}}} \qquad \text{Equation 3-8}$$

If the Venturi tube is located at the collector outlet (high temperature), then T_{out} is used in the denominator of Equation 3-8, and if at the inlet, T_{in} is used.

This brings about the simple question of where the flow should be measured with a Venturi nozzle. By inspecting Equation 3-8 it can be seen that the denominator will change by a factor of the square root of the temperature while the numerator remains constant. Dividing by T_{out} for the outlet (the highest system temperature) by T_{in} for the inlet (the system's coolest temperature) gives the ratios $\frac{[\frac{\partial \eta}{\partial \Delta P_V}]_{out}}{[\frac{\partial \eta}{\partial \Delta P_V}]_{in}} = \sqrt{\frac{T_{in}}{T_{out}}}$.

Typical values might be T_{in}= 80°F = 540°R and T_{out} = 140°F = 600°R. Inserting these values into the equation yields $\frac{[\frac{\partial \eta}{\partial \Delta P_V}]_{out}}{[\frac{\partial \eta}{\partial \Delta P_V}]_{in}} = \sqrt{\frac{540}{600}} = 0.95$. The conclusion regarding Venturi tube measurement error is that the nozzle will manifest approximately a 5% less error if it is located at the hot outlet, instead of the inlet. This seems reasonable; logic indicates that for a given flow rate, the density is diminished at the hot outlet, so the velocity (V) and therefore the ΔP_V readings will be greater, and larger readings are less prone to percentage error.

<u>Hand-Held Velocity Meter Mathematical Development</u>

If a hand-held air velocity meter directly reads the air velocity, then in Equation 3-1 $Q = A_D * V$ and Equation 3-7 is modified to Equation 3-9.

$$\eta = \frac{K_M \; P_A \; V\,(T_{out} - T_{in})}{I\,T_{out\ or\ in}} \quad where\ K_M = \frac{A_D \; c_p}{A_c \; R_{air}}$$ Equation 3-9

Equation 3-9 is the equation to be analyzed in the sensitivity analysis when using a direct velocity measurement device. Note all parameters are linear, as opposed to Equation 3-7. Proceeding as above yields, $\frac{[\frac{\partial \eta}{\partial V}]_{out}}{[\frac{\partial \eta}{\partial V}]_{in}} = \frac{T_{in}}{T_{out}} = \frac{540}{600} = 0.90$

This suggests that for the direct velocity measurement, a reading taken at the hot exit is subject to about a 10% less percentage error than one taken at the cool inlet. However, if possible the hand-held instrument should take readings at both the inlet and outlet to serve as a veracity check.

In a working SBAC, where flow measurements are not taken and only long term performance is of concern, there are several advantages to having the blower pressurize the system by blowing into the inlet, rather than drawing from the outlet.

Since most site constructed units are large and have leaks, pressurization tends to blow dust and detritus out of leaks in the collector, whereas suction at the outlet would tend to draw particulates into the system. Also, many blowers have built-in thermal protection, which turns the motor off if the temperature rises above the motor design point, often set at 104^{o}F = 40^{o}C. Sucking hot air into the blower may trigger the thermal protection shut off, whereas drawing cooler air into the blower minimizes the possibility of downtime due to thermal disconnect, especially in winter.

A given blower will move a greater mass flow rate of cool higher density air relative to warmer air, because the motor moves the rotors at a certain rpm and produces a certain volumetric flow rate, regardless of air density. Therefore, the cooler the air, the greater the mass flow rate, for a given blower and power consumption, which is a compelling reason to locate the blower at the collector inlet for a working system.

Two general observations should be noted with Equation 3-9. Although the values for the constant K_M are simple to measure accurately; the constant will change for each collector test. This is because the factor K_M in the denominator contains the area of the collector, which can reasonably fluctuate by a factor of 5 for differing collector sizes. This will have a linear impact in measuring efficiency. Consequently measuring larger collectors will inherently be more accurate than measuring smaller collectors. Equation 3-9 has even more variability, as the size of the duct where the velocity is measured has a further impact as a smaller duct will increase the velocity speed measured. A given error sustained while measuring a low speed is more significant percentage wise than the same error made measuring a higher speed. Therefore it is preferable that the velocity measured will be from the smallest duct feasible. Finally the specific heat of air (Cp) is a weak function of temperature. For the temperature ranges that collectors will be tested this variation will be too small to have an impact on the specific heat. So, this as well as well as the universal gas constant (R_{air}) are considered constant for all tests.

Sensitivity Test

Now that the required equations and theory for a Venturi Nozzle (Equation 3-8) and a hand held flow meter (Equation 3-9) have been developed, a complete sensitivity test can be performed to determine how much measurement errors will affect the final estimated efficiency. Expanding on the methods described previously to the remaining parameters listed in Equation 3-10 and Equation 3-11 can be developed for a Venturi Nozzle and a hand-held flow meter, respectively. A final sensitivity test was conducted and the total error in measurement was estimated for both methods of calculating flow. These errors are tabulated in Table 3-1 and Table 3-2 using observed values during the Goldade SBAC test (see chapter 7). It is clear from Tables 3-1 and 3-2 that although the Venturi Tube is inherently more accurate than the hand held velocity meter, both are reasonably accurate for engineering testing.

Venturi Tube Error Analyses:

$$\frac{\Delta\eta}{\eta} = \frac{1}{\eta} * \left(\left[\frac{\partial\eta}{\partial P_V} * \Delta P_V\right]^2 + \left[\frac{\partial\eta}{\partial P_a} * \Delta P_a\right]^2 + \left[\frac{\partial\eta}{\partial T_{out}} * \Delta T_{out}\right]^2 + \left[\frac{\partial\eta}{\partial T_{in}} * \Delta T_{in}\right]^2 + \left[\frac{\partial\eta}{I} * \Delta I\right]^2\right)^{1/2}$$

Equation 3-10

Where:

$$\frac{\partial\eta}{\partial P_V}\Delta P_V = \frac{K_V\sqrt{P_a} * (T_{out} - T_{in})}{2 * I * T_{out}\sqrt{P_V}} * \Delta P_V$$

$$\frac{\partial\eta}{\partial P_a} * \Delta P_a = \frac{K_V\sqrt{P_V} * (T_{out} - T_{in})}{2 * I * T_{out}\sqrt{P_a}} * \Delta P_a$$

$$\frac{\partial\eta}{\partial T_{out}} * \Delta T_{out} = \frac{K_V\sqrt{P_a}\sqrt{P_V} * T_{in}}{I * {T_{out}}^2} * \Delta T_{out}$$

$$\frac{\partial\eta}{\partial T_{in}} * \Delta T_{in} = -\frac{K_V\sqrt{P_a}\sqrt{P_V}}{I * T_{out}} * \Delta T_{in}$$

$$\frac{\partial\eta}{\partial I} * \Delta I = \frac{K_V\sqrt{P_a}\sqrt{P_V} * (T_{out} - T_{in})}{I^2 * T_{out}} * \Delta I$$

Hand Held Flow Meter Error Analyses:

$$\frac{\Delta\eta}{\eta} = \frac{1}{\eta} * \left(\left[\frac{\partial\eta}{\partial V} * \Delta V\right]^2 + \left[\frac{\partial\eta}{\partial P_a} * \Delta P_a\right]^2 + \left[\frac{\partial\eta}{\partial T_{out}} * \Delta T_{out}\right]^2 + \left[\frac{\partial\eta}{\partial T_{in}} * \Delta T_{in}\right]^2 + \left[\frac{\partial\eta}{I} * \Delta I\right]^2\right)^{1/2}$$

Equation 3-11

Where:

$$\frac{\partial\eta}{\partial P_a} * \Delta P_a = \frac{K_V * V * (T_{out} - T_{in})}{I * T_{out}} * \Delta P_a$$

$$\frac{\partial\eta}{\partial V} * \Delta V = \frac{K_V * P_a * (T_{out} - T_{in})}{I * T_{out}} * \Delta V$$

$$\frac{\partial\eta}{\partial T_{out}} * \Delta T_{out} = \frac{K_V * V * P_a * T_{in}}{I * {T_{out}}^2} * \Delta T_{out}$$

$$\frac{\partial\eta}{\partial T_{in}} * \Delta T_{in} = \frac{K_V * V * P_a}{I * T_{out}} * \Delta T_{in}$$

$$\frac{\partial\eta}{\partial I} * \Delta I = \frac{K_V * V * P_a * (T_{out} - T_{in})}{I^2 * T_{out}} * \Delta I$$

Table 3-1: Error List for a Venturi Nozzle

Standard Error Venturi Tube					
Variable x_i	Instrument error	Standard Value	Error	$\delta\eta/\delta x_i$	$\delta\eta/\delta x_i^2$
Pa (Kpa)	0.32%	85.5	0.2736	0.09%	0.000%
Pv (Kpa)	1.00%	0.25	0.0025	0.27%	0.001%
T_{out} (^oK)	0.30%	333	1	0.01%	0.000%
T_{in} (^oK)	0.33%	303	1	-1.80%	0.033%
I (W/m^2)	1.00%	1000	10	0.54%	0.003%
				Sum$^{0.5}$	**1.91%**

Table 3-2: Error List for Hand Held Flow Meter

Standard Error Velocity Meter					
Variable x_i	Instrument error	Standard Value	Error	$\delta\eta/\delta x_i$	$\delta\eta/\delta x_i^2$
Pa (Kpa)	0.32%	85.5	0.2736	0.00%	0.000%
Vel (m/s)*	3.00%	2	0.06	1.20%	0.014%
T_{out} (^oK)	0.30%	333	1	1.21%	0.015%
T_{in} (^oK)	0.33%	303	1	1.34%	0.018%
I (W/m^2)	1.00%	1000	10	0.40%	0.002%
				Sum$^{0.5}$	**4.41%**

Chapter 4. Development of a Mobile Solar Evaluation Laboratory (MSEL)

A primary objective of this thesis is to design, construct and validate a portable testing unit and procedure capable of producing a SBAC efficiency curve in an expedient and efficient manner in the field. This by definition would be a modular unit capable of portably testing any collector in one session, over a period of a few hours, provided the weather was conducive to solar testing. This strongly differs from SRCC solar ratings as their rating process is rigorous, detailed, the collector must be oriented normal to the sun, and time consuming. It is not uncommon for a SRCC rating of a solar thermal collector to take over 6 weeks because of the stringent standards by which they abide. These standards render the rating of SBACs to SRCC specifications impractical, as it would likely require a specialized team to test the collector over a period of weeks, waiting for perfect weather conditions; often in winter. Furthermore, SBACs are by definition immobile; so, should the construction of the collector be built in a way to where it is never normal the sun, it would be impossible to test this collector as per SRCC standards. The cost associated with this type of testing will always be unrealistic. Currently, any governmental or private incentives for thermal collectors must be rated by the SRCC first (U.S Department of Energy, 2015). This makes any SBAC infeasible to incentivize and less attractive to home owners and contractors alike, despite the fact that, the cost/ft^2 for SBACs is typically a fraction of that of their modular counterparts and their performance is often comparable to commercially installed units.

The reasons listed in the previous paragraph led to motivation of the design and construction of the Mobile Solar Evaluation Laboratory (MSEL). It is intended that a portable unit could quickly and accurately obtain data required to develop an efficiency curve that would be comparable to what the SRCC develops. It would also follow the specifications outlined by both ASHRAE and SRCC when feasible. The MSEL will have the following advantages over an SRCC-generated curve, provided the results generated from the MSEL were indeed accurate.

1. It will be feasible to test Site Built Air Collectors: If testing can be reliably administered, it can potentially open up an entirely new market for renewable energy careers. These careers could be private companies or managed directly by the incentive provider.
2. It will be inexpensive in both man-hours and equipment: Testing with the MSEL will take only a few hours on an acceptable solar day. Furthermore the testing procedure outlined is relatively simple to follow, meaning there is no need for highly skilled labor to operate the unit; technicians will be trained to operate the MSEL and evaluate stationary systems. Nor is there a need for a standardized laboratory. Also the time required for testing will be a fraction of that the SRCC requires. The collected data will be input into a laptop computer and the solar system performance curve will be generated in the field. Then the technician can issue a Certificate of Compliance directly to the

homeowner during his/her visit, which the client can then present to the inducement provider. Finally the SRCC testing protocol involves extensive and complex operations. The MSEL by comparison is an inexpensive and simple unit. These factors should drive the cost for testing an air collector (both site-built and modular) down to affordable prices for homeowners.

3. The ability to test collectors at low cost: The current method for testing a collector by the SRCC is to select a random collector from the factory floor. This method has several complications. First, statistically speaking, this is an invalid method to test a solar collector population, as the sample size is insufficient garner an accurate estimate of the population's performance. This is especially true for small companies who may not have sufficient quality control in their products. Second, they only test new collectors, while typical air collectors are in operation for several years. This means the curve they produce is only relevant before the collector starts to degrade; currently there are no testing procedures for collectors after years of use.
4. The MSEL will allow testing under realistic conditions: The curves generated are dependent on the ambient testing conditions. For example, if the ambient conditions have low temperatures and high winds, the efficiency curve will be less favorable than a curve that was developed in high temperatures and low winds. Finally the collectors that are tested at SRCC are meticulously looked after to ensure ideal insulation and no leakage of the collector or duct system.

Conversely, in practice, air collectors are prone to leakage, and are often prone to heat losses due to installation errors. The MSEL will detect these errors and create a realistic curve for the collector system (not just the collector) on that day. In contrast, the SRCC will develop a curve for the collector that they tested, under ideal conditions, typically during the summer months when space heat is not utilized. One could easily make the argument that if an efficiency curve could be accurately generated from the MSEL, this curve would be more applicable to the heat savings in real-world situations than that generated by the SRCC.

5. Finally, the MSEL would allow for multiple tests, thereby enabling determination of system degradation over time. This may allow for improved incentive policies to take into account collectors that maintain efficiency curves over longer periods of time.

Figure 4-1 and Figure 4-2 show the MSEL. These figures reveal the unit is quite small and easily fits in the back of a pickup or SUV.

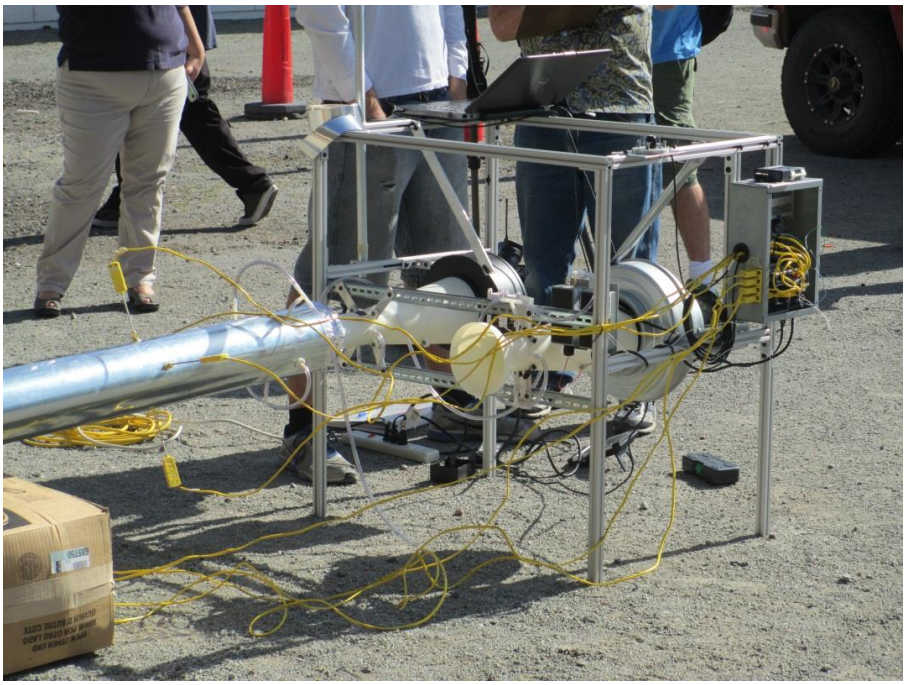

Figure 4-1: MSEL

Figure 4-2: MSEL and Collector

As previously stated, the goal of the MSEL is to accurately and inexpensively develop efficiency curves for SBACs. To do this it is deemed most convenient to record, by hand, all applicable data during steady state conditions and evaluate it in Excel for immediate analysis. This will allow for the efficiency curve to be produced in the field, and should the curve meet the set standard, a Certificate of Compliance can be issued to the client.

The next section will state what equipment and methods are utilized to measure the required variables listed in Chapter 3.

Insolation- Insolation is measured with an Apogee pyranometer model number SP-215/AL-100 in the units of W/m^2. The pyranometer was mounted directly on the surface of the collector being tested to obtain the most accurate measurement of Insolation.

Intake and Outtake Temperature- The intake and outtake temperatures are measured with four Omega KQSS-18E-6 iron constantan thermocouples placed orthogonal to each other on the intake and outtake ducts as is shown in Figure 4-1, approximately 1" deep in the ducts. The data are recorded in ^oC and the four readings for the intake and outtake are averaged for the calculations described in the previous chapter. Small holes were drilled into the ducts in accordance with ASHRAE. To prevent leakage once the thermocouples were placed in the ducts, the holes were sealed with duct tape.

Ambient Temperature- Ambient temperature was measured by a Digikey MCP9701-E/TO-ND. It should be noted that for accurate readings, the sensor must be placed in the shade in the vicinity of the collector.

Pressure at the Throat Nozzle and in Intake and Outtake Ducts- Pressure is measured by taking the average of four pressure readings located orthogonal to each other in both the nozzle throat and the intake duct. For the nozzle, the pressure taps were part of the structure and pressure tubes could be placed directly on the taps. For the ducts, pressure was measured at the location as described by ASHRAE standards. Small holes were drilled and rubber gaskets were attached to the pressure tap using duct tape to prevent as much leakage as possible. The pressure was measured with four Omega PX274-05DI pressure transducers.

Time of Day- The time of day is noted during every recorded measurement.

Ducts- For flexibility and portability two 10’ long, 6” diameter metal ducts are attached to the pressure nozzles, in accordance with ASHRAE standards for both the intake and outtake of the collector tested. These ducts were insulated with R-15 insulation to prevent heat transfer to or from the ambient conditions. To connect the metal ducts to the intake or outtake of the collector, R-15 insulated flex ducting was utilized. The connections from duct to flex duct and flex duct to collector were duct taped to ensure minimal flow losses.

Weather Conditions- The weather conditions are measured with a WS-2090 Ambient Weather wireless home weather station. This measures the relative humidly,

wind speed and direction, and ambient temperature, among other conditions. These data are utilized in post-analysis to determine if the weather conditions were relatively constant.

Ambient Pressure- The ambient pressure is measured via Omega EWS-BP-A. The data are recorded at the beginning of the test and once every hour.

Structure- The framing structure to hold the weather station, blower, duct works, nozzles, DAQ, and Laptop was a standard McMaster 47065T101 frame.

Blowers - Should the air collector being tested not have its own blower, or the blower is inaccessible, the MSEL includes two blowers to allow for testing. A Dayton/Grainger 1TDV4, and a Grainger 4YM45, FG8XL blowers rated at 310 and 502 cfm, respectively, at no load, are attached to the structure. These blowers allow for differing sized collectors to be tested and maintain the recommend flow rate to area ratio of 2 to 6 ft/min (Solar Rating & Certifiaction Corporation, 2014).

Measuring Flow Rate

With the required equipment established, the air flow rate through the collector must be ascertained. To measure flow rate, standard ASHRAE 93-2010 was reviewed. The duct flow configuration described in this standard was deemed to be the most practical and relevant for measuring flow rate in a modular manor. As a result, the MSEL was modeled after this configuration.

The flow rate is measured by the pressure differential across the throat of a nozzle and appending duct. Two 3” diameter throats expanding to 6” flaring diameter

nozzles were built via a 3-D printing machine at UNR in accordance with the standards outlined for nozzle configuration in ASHRAE 93-2010. Pressure taps were constructed into the throat in four orthogonal locations. On the other end of the nozzle a transformer was attached to expand the throat at a 7^{o} angle to a 6.3" diameter. This was done so the nozzle could be seamlessly connected to most blowers. Figure 4-3 shows an isometric 3-D view of the nozzle design complete with pressure taps, designed using the mechanical 3-D CAD program, Solid Works.

The pressure taps (Figure 4-4) and transformer were also designed in accordance to ASHRAE 93-2010; Figure 4-5 shows an Isometric view of the transformer piece. The entire nozzle configuration (complete with transformer and pressure taps) was assembled in 3 parts, for flexibility. Should an air blower require a different dimension nozzle, the transformer piece(s) can be removed and another nozzle could be attached, if needed. Figure 4-6 shows the finished nozzle/transformation piece. As can be seen in Figure 4-1 the nozzle is connected to the metal duct with duct tape to prevent leakage with the blower placed directly behind a transformation piece. This piece fits the diameter of blowers of the MSEL to ensure minimal leakage and maximum airflow. The equations listed in the sensitivity test were modified from ASHRAE 93-2010, as explained in next section. These equations were utilized to calculate the flow rate and collector efficiency from the data acquired.

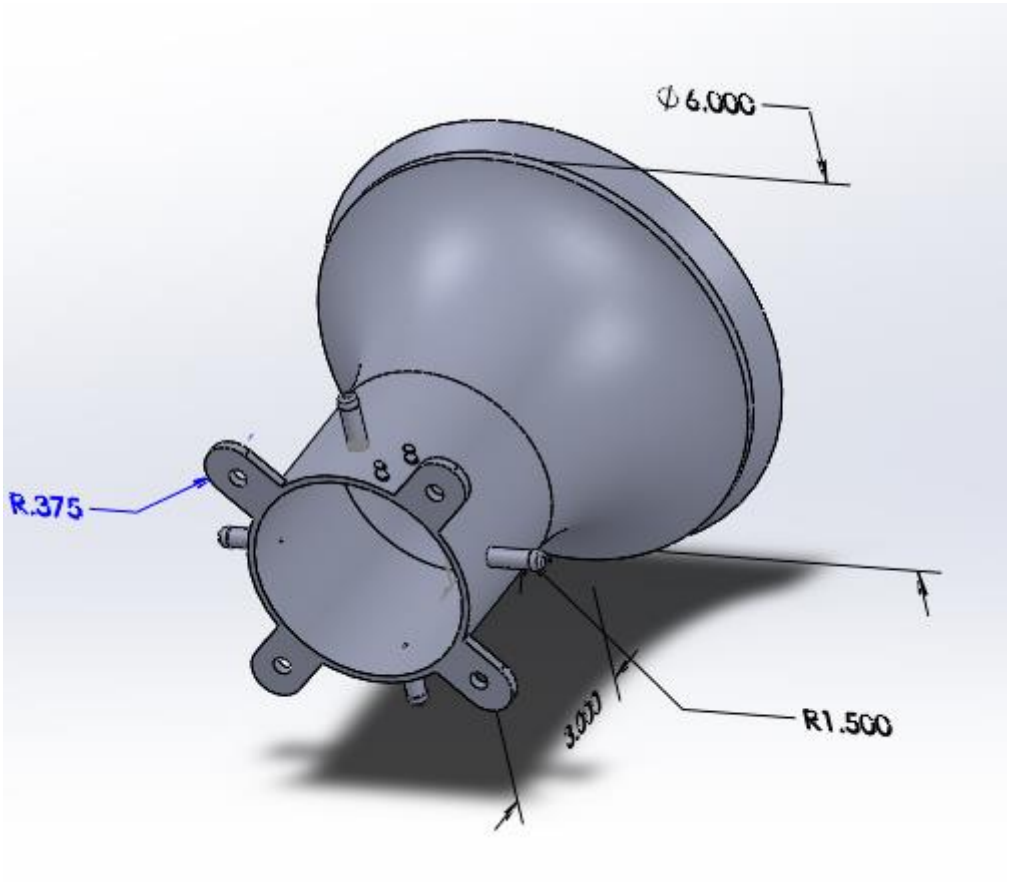

Figure 4-3: Solid Works 3'' Throat Nozzle Design with Taps

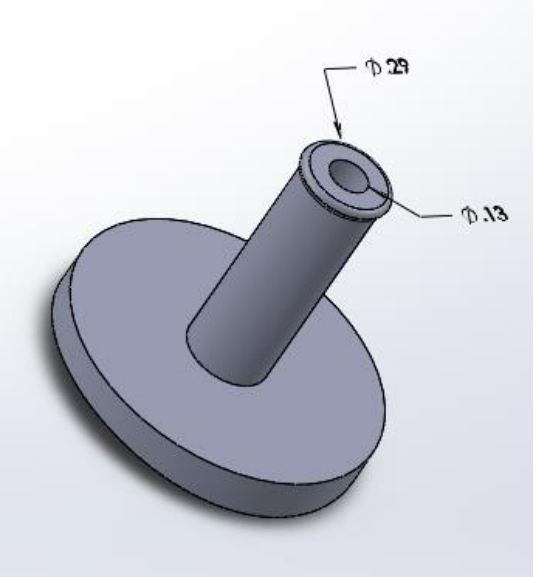

Figure 4-4: Tap Pressure Design

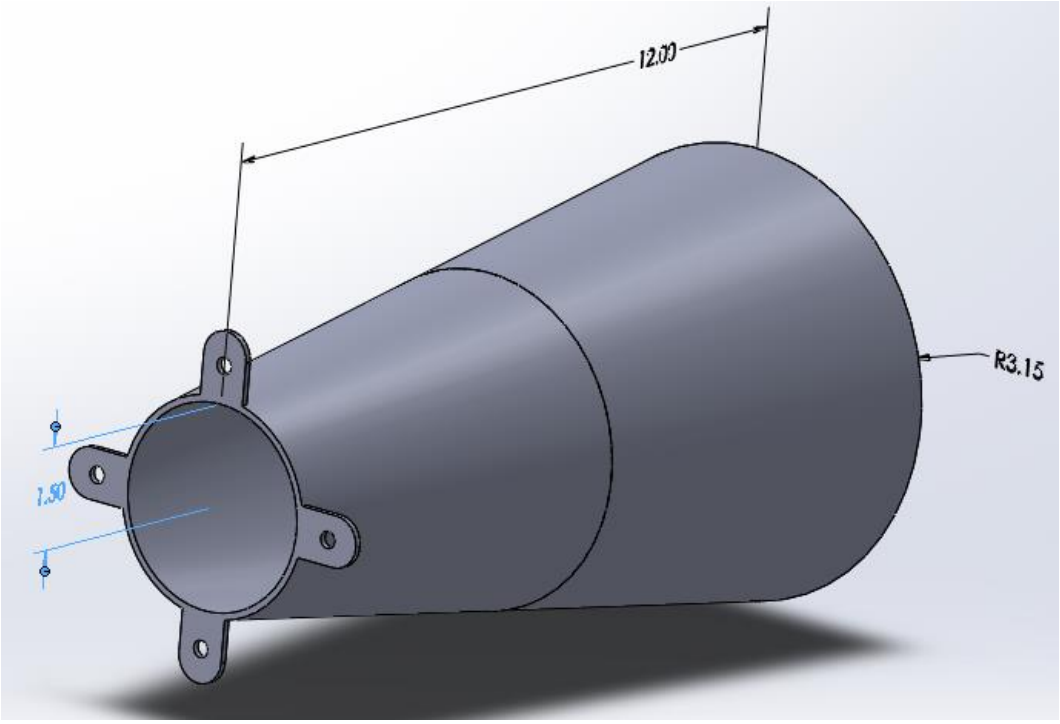

Figure 4-5: Transformer Piece

Figure 4-6: Completed Nozzle Design

A: Pressure taps
B: Mounting tabs
C: Nozzle throat
D: Duct connection

4-7: Duct Configuration

A: Thermocouple probes
B: Thermocouple taps
C: Pressure taps
D: Pressure manifold

An alternative method to measure air volumetric flowrate is to directly measure air velocity in either the collector intake duct, exit duct, or both. To develop a more economical and practical testing unit, tests were conducted that utilized a simple hand held air flow meter, such as the unit shown in in Figure 4-8. These tests showed the flow rate obtained from the simple air flow meter were within an acceptable tolerance when compared to that of a standard Venturi tube.

These commercial alternatives are within the permissible accuracy of 1.5%, as defined by ASHRAE, and are a viable alternative to the complex airflow measurement devices such as the configurations described by their standards. These flow meters are portable, low cost, convenient, and are reasonably accurate for field test conditions.

Figure 4-8: Commercial Air Flow Meter

Using a unit such as is shown in Figure 4-8 would have a drastic impact on the ease of taking flow rate measurements in the field, as these units are not limited by flow speed (ASHRAE duct configuration requires the flow to be between 3000 ft/min to 7,000 ft/min to employ the Venturi nozzle (ASHRAE, Standard 93-2010, 2010). The system described by ASHRAE is cumbersome and requires greater time for set up, and the equipment required to measure the requisite inputs are expensive. This makes the use of air flow meters in the field more practical and economical. Finally, the Venturi tubes and duct system created proved a fragile design, which required constant maintenance.

To test the applicability of utilizing a simple flow meter as opposed to the complex requirements described by ASHRAE, tube flow rates were compared utilizing the two differing methods described. Testing was conducted at Dr. Turner's house in July, 2015. It was found that the flow rates measured with the differing methods yielded a difference of less than 5%, when utilizing the pumps of the MSEL. Furthermore it was found that the temperature read-out on the hand-held flow meter and thermocouples of the MSEL were also in agreement with differences of less than 3%. This proves the utility of a simple flow meter over the more complex and cumbersome Venturi tube.

MSEL Set-Up & Data Handling

This section will briefly describe the test day procedure. Figure 3-1 shows a general schematic of the airflow for the MSEL. Air will be blown out of the collector, and a flex duct connects the outlet to the inlet via a butterfly valve. Modifications of the

butterfly valve settings allow for differing inlet temperatures required for collector testing.

The comprehensive idea for testing a SBAC is to simply measure the operating conditions after 15 minutes, or after the variations in outlet temperature have visibly stabilized from the read out of the MSEL, whichever is greater, for each intake temperature. Once these conditions have been met, the current collector conditions would be in or close to steady state (as required by ASHRAE to record data). After this, the intake temperature is incrementally increased until it is equal to the exit temperature (this condition is called stagnation).

The stagnation condition is obtained by closing the butterfly valve to ensure no ambient air is introduced into the system. This ensures that $T_{in}=T_{out}$ and the collector is producing no useful heat (this produces the x-abscissa on Figure 3-2), and corresponds to zero collector efficiency. The ordinate of the efficiency-flow/parameter curve (the y-ordinate on Figure 3-2) is found when the butterfly valve is completely open. This ensures $T_{in} = T_{amb}$. Intermediate points are found by blending differing amounts of ambient and heated air into the system via the butterfly valve. With each change in intake temperature, the data from the MSEL are recorded after the outtake temperature has stabilized.

If the intake temperature starts at ambient and ends at the stagnation temperature, this will provide sufficient data to generate an accurate efficiency curve. The 15-minute tests would be implemented over a wide inlet temperature range to

capture as many sections of the efficiency curve as possible. If time permits, the inlet temperatures will be repeated several times during the test to allow for multiple data points at differing times. It should be noted that the resins utilized in the nozzle pieces are only rated for 100 ^{o}C. As such, care must be taken to ensure the inlet and outlet temperatures would not exceed this rated temperature.

The angle of incidence (θ) is calculated using the tilt of the collector (measured on site) and the methods described in Chapter 5. This is an important characteristic of solar testing as the angle of incidence will impact the transmissivity of the glazing material. For a further explanation see Chapters 5 and 7 for the theoretical calculations and an example of how the transmittance changes with changing angle of incidence.

Finally, it is pertinent to discuss a quick and effective way to field-generate a curve, by simply drawing ambient air into the collector to generate several data points on the ordinate of the efficiency-flow/parameter curve. During these runs the flowrate is established, because measurements can be taken at both the inlet and exit. The hot exit flow is then ducted to become the inlet, so the system is running at hot-maximum stagnation condition. It will not be possible to insert the handheld velocity meter, so the velocity will be assumed the same as for the free flowing system. This should not introduce much error with short insulated large flex ducts (such as the ones utilized during testing). For this condition the efficiency is zero, and the exit-inlet (same) air temperature will give the flow parameter $(T_{in}-T_{amb})/I$, and several points will be plotted on the curve abscissa. Drawing a straight line between the two groups of points

provides a quick and reasonably accurate performance curve which should be sufficient to establish whether or not the system is working to a preset required standard. This bypasses the laborious and time-consuming process of acquiring diffing inlet temperatures data points. Furthermore, this drastically reduces testing time and costs associated with equipment and labor.

Chapter 5. Field Testing and Validation of the (MSEL) on Goldade Collector

The development and construction of the MSEL was described in Chapter 4. It was demonstrated that a handheld velocity meter could provide equivalent results to a Venturi nozzle, which facilitates air flowrate measurement, a result that simplifies the MSEL and reduces its utilization expense.

Anticipating this thesis, the Goldade Family constructed a 128 ft^2 (115 ft^2 active surface) solar collector at their home in Minden, Nevada, for the purpose of heating their house in winter (see Figure 5-3). The MSEL was employed to determine the Goldade Collector's performance constants. Also, as a verification of the MSEL, the steady state empirical data were compared a theoretically predicted curve of the Goldade collector. Close correlation was achieved.

The first part of this chapter develops the efficiency versus flow parameter curve from theory for a Goldade class collector. The second part documents the MSEL tests that lead to an empirical performance curve. Comparing the two curves gives gratifying assurance that theory and field testing are reasonably close. The measured parameters also provide the coefficients needed to conduct the technical and economic analysis in Part 2 of this thesis.

Goldade Collector Theoretical Analysis

It is necessary to develop a mathematical method to determine theoretical steady state efficiency curves. Then we can compare theoretical performance

estimates to observed performance for several systems. There are several factors that influence the collector perfomance. The most improtant are the collector location, orientation, the day when the collector is in use, the collector type and the test conditions. A change to any of these variables will change (sometimes drastically) the performance of the collector.

Solar Angle of Incidence (θ): It is necessary to determine the exact orientation of the collector relative to the sun at any given time. This will take into consideration the longitude, latitude, collector tilt, time of day, and date of the collector is in use. The angle between the collector surface normal and beam radiation (θ) can be found with Equation 5-1 (Duffie & Beckman, 1980).

$$cos\theta = \sin\delta sin\varphi cos\beta - sin\delta cos\varphi sin\beta cos\gamma + cos\delta cos\varphi cos\beta cos\omega + cos\delta sin\varphi sin\beta cos\gamma cos\,\omega + cos\delta sin\beta sin\gamma sin\omega \qquad \text{Equation 5-1}$$

Where:

θ = Angle of incidence between sloped collector and normal incoming beam radiation

δ = Declination angle

φ = Latitude of the collector

β = Slope of the collector form horizontal

γ = Angle of collector from due south

ω = Hour angle for each hour before and after solar noon this will equal -15^o and 15^o respectively

Θ is needed for the calculation to make two corrections. First, if the MSEL is evaluating a collector, then the transmissivity (τ) correction must be made, or the efficiency will appear to be artificially low. The τ correction, and how it was accounted for in MSEL testing is discussed towards the end of the chapter.

Second, if we do not have a direct normal value for insolation then we must multiply the insolation value by cosine Θ to account for the direct beam actually incident on the collector. Generally this is not a problem because the pyranometer is mounted flush with the collector surface, so the actual total incident insolation is directly recorded.

General Solar Collector Efficiency Equation: The methodology for conducting a steady state analysis on a flat plate solar collector has been provided by standard thermal collector analysis, with modified estimates of convection heat transfer coefficients utilized (Duffie & Beckman, 1980), (Cengel & Turner, 2001). This analysis determines the required parameters to develop theoretical efficiency curves that can be compared to the curves developed during field studies. The required collector characteristics for these curves are the transmissivity (τ), absorptivity (α), total heat loss coefficient (U_L), the heat removal factor (F_R) and the efficiency factor (F'). The normal-incident transmissivity and absorptivity are typically known or can be assumed; the

remaining factors are dependent on the collector type and ambient conditions, so they must be analytically determined.

The SBAC featured in this study has a single fiberglass glazing mounted on top of two channels. Half way between the glazing and the insulated back wall is a black absorber. Air flows on both sides of the absorber to collect heat absorbed from the sun. A side view schematic of the system, showing thermal resistances, is given in Figure 5-1. Table 5-1 shows the geometric parameters of the collector.

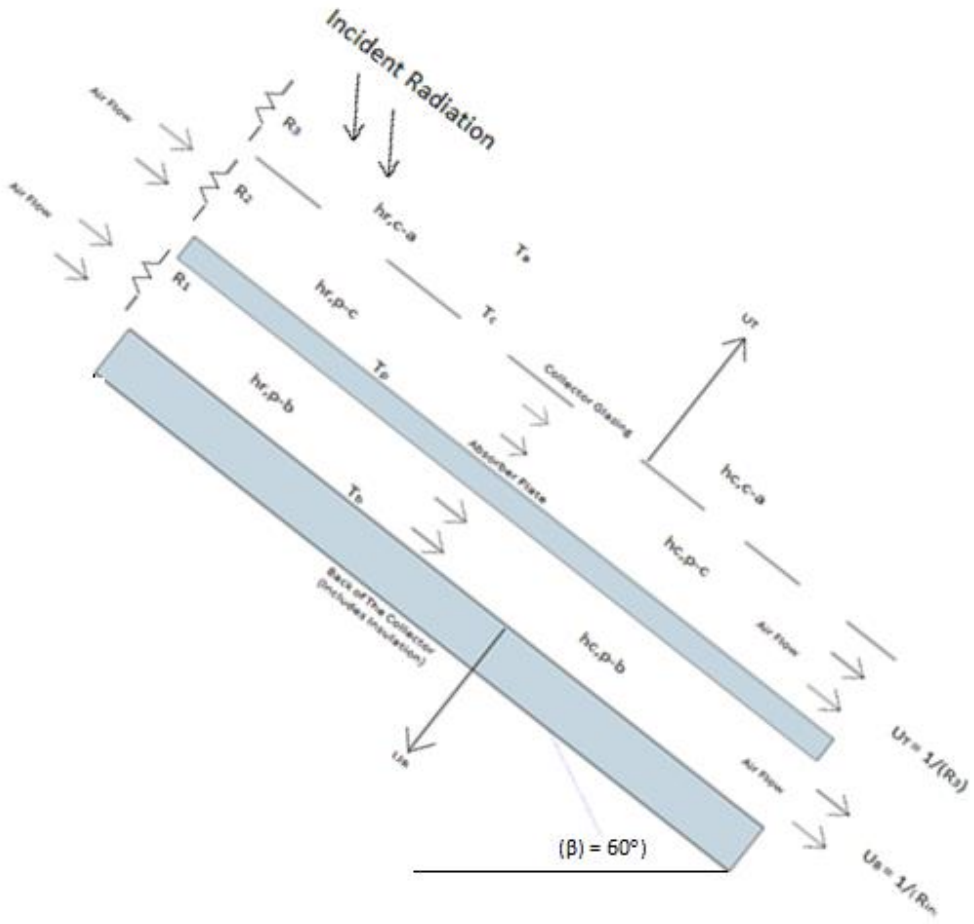

Figure 5-1: Geometry and heat transfer coefficients for the Goldade Collector

Table 5-1: Collector Dimensions

Goldade Collector Dimensions		
Area *	128	(ft^2)
Length	16	ft
Width	8	ft
Air Channel width	4	in
Hydraulic diameter (D_H)	7.65	in

*Note the active area is 115 ft^2

It should be noted that air which flows above the absorber also flows on the underside of the glazing, which promotes heat loss from the collector. This loss consists of two components, (1) the linearized radiative loss coefficient $h_{r,\ p\text{-}c}$, and (2) the convective loss coefficient $h_{c,\ p\text{-}c}$.

The general efficiency curve is determined from basic heat transfer and the analysis, and is defined in Equation 5-2 (Duffie & Beckman, 1980).

$$\eta = \frac{Qu}{A_c * I} = F_R(\tau\alpha) - F_R U_L * \frac{T_i - T_a}{I} \qquad \text{Equation 5-2}$$

Where:

Qu = Useful heat output of the collector (W)

F_R = Heat removal factor (Unitless)

U_L = Overall heat transfer coefficient (W/m^2-^oC)

T_i and T_a = Temperature in the inlet and ambient respectively (^oC)

I = Solar radiation striking collector surface (W/m^2)

τ = Transmissivity of the glazing material (Unitless)

α = Absorptivity of the absorber surface (Unitless)

Note the definition of efficiency has been developed in the form of y = mx + b. By setting the ambient temperature to that of the inlet temperature the "y-intercept" for the efficiency curve can be found as $\eta = F_R * \alpha\tau$. And since τ and α are readily known, the heat removal factor F_R is proportional to the y-intercept value.

During testing, if the hot air flow exiting the collector is immediately routed to become the collector air intake, then the collector efficiency eventually will become zero as no useful heat will be produced. This is called the stagnation condition, and represents the collector operating at its maximum temperature for the given conditions. Zero efficiency is consistent with the efficiency equation x-axis intersection. For η = 0 Equation 5-2 becomes

$$\frac{T_i - T_a}{I} = \frac{\alpha\tau}{U_L} \qquad \text{Equation 5-3}$$

Equation 5-3 provides a convenient way to measure U_L in the field, since all other parameters are known or easily measured.

When the x-coordinate is taken to be "Flow Parameter" $(T_{in} - T_{amb})/I$, then the slope of the efficiency curve Equation 5-2 is equal to $-F_R U_L$.

Determining U_L: Strictly speaking, the process of determining U_L is iterative, because the temperatures of the plate, cover, back and air at a given location are unknown, and the heat transfer coefficients are weak functions of these temperatures. However, in actual practice, the temperatures can be assumed, from which the various coefficients can be accurately determined, leading the overall heat loss coefficient U_L. Although U_L for several geometries are listed in the literature, U_L for the geometry indicated in Figure 5-1 was not found in a convenient form, so it is developed below.

The absorber is the hottest point in the thermal system, because most of the solar radiation that has transmitted through the glazing is absorbed here. The absorber is sufficiently thin at a given location it is considered isothermal. The air flowing on both sides of the absorber is heated by convection, per design. However, the heated air also contacts the cooler glazing above, and heat lost to the glazing is lost from the system to the ambient environment. There is also a radiative transfer between the hot absorber and cooler glazing. The sum of the convective and radiative heat losses to the environment constitutes the top loss coefficient U_T.

On the other side of the absorber, both convection and radiation from the absorber to the back wall, and then by conduction through the back insulation, constitutes the back loss coefficient U_B. Note, if the collector were built onto a (insulated) house wall where winter heat is needed, the back loss coefficient will be

zero. This is because heat that does pass through the back of the collector is transferred into the house, where it is utilized for winter space heating.

The overall heat loss coefficient can be described as the following simplistic equation: $U_L = U_T + U_B$. The thermal resistances due to convection (nearly linear) and the linearized radiation losses are mathematically similar to electrical resistances. Thus, for convection from the absorber to air, or from air to glazing, the standard equation is defined as $Q = h*A(T_P - T_{air})$, which can correctly be rewritten as $Q = (1/R)*A(T_P - T_{air})$; conductance is defined as $h = 1/R$, with R the being thermal resistance.

In Figure 5-1 for heat to transmit from the absorber to the glazing cover (or to the back) by convection, the heat first is lost by convection to the air, then from the air to the next surface. As a result, there are two convective resistances. Because the average fluid temperature will not vary drastically it will be assumed that the convection coefficient for the front will equal that of the back. Radiation between two close parallel infinite plates is given by:

$$Q_{rad} = \frac{\sigma(T_p^4 - T_c^4)}{\frac{1}{\varepsilon_p} + \frac{1}{\varepsilon_c} - 1} = \frac{\sigma(T_p^2 + T_c^2)(T_p + T_c)(T_p - T_c)}{\frac{1}{\varepsilon_p} + \frac{1}{\varepsilon_c} - 1}$$ Equation 5-4

Where:

σ = Stefan Boltzmann constant ($5.67*10^{-8}$ W/m^2-^{o}K^4)

T_p and T_c = Temperatures in degrees absolute of the absorbing surface and glazing cover respectively (°K)

ε_p and ε_c = Emissivities of the absorbing surface and glazing cover respectively (Unitless)

Equation 5-4 can be rewritten as $Q_{rad} = h_r(T_p - T_c)$. Where h_r is a linear form of radiative heat transfer, which is similar to convection. Thus:

$$h_{rad} = \frac{\sigma\left(T_p^2 + T_c^2\right)(T_p + T_c)}{\frac{1}{\varepsilon_p} + \frac{1}{\varepsilon_c} - 1} \approx \frac{4\sigma T_{Ave}^3}{\frac{1}{\varepsilon_p} + \frac{1}{\varepsilon_c} - 1} \qquad Where\ T_{Ave} = \tfrac{1}{2}(Tp + Tc) \quad T = {}^{\circ}Absolute$$

Equation 5-5

Note: The thermal resistance due to radiation (R_{rad}) can be defined as $R_{rad} = 1/h_r$

Equation 5-5 shows that the average of T_P and T_c (in absolute temperatures) need to be known for a precise estimate, which would entail an iterative process. However, the result is not sensitive to moderate temperature changes, so acceptable accuracy is achieved by assuming reasonable temperatures.

Since radiation and convection occur in parallel, one can combine these resistances to one overall resistance for the thermal network absorber and top cover. Recalling that for parallel resistances reciprocals are additive, Equation 5-6 is obtained:

$$\frac{1}{R_{p-c}} = \frac{1}{R_{conv}} + \frac{1}{R_{rad}}$$ Equation 5-6

Where:

R_{p-c} = Thermal resistance network of the plate to cover ($^oC\text{-}m^2/W$)

R_{conv} = Thermal resistance due to convection between the plate to cover ($^oC\text{-}m^2/W$)

R_{rad} = Thermal resistance due to radiation between the plate to cover ($^oC\text{-}m^2/W$)

Equation 5-6 is valid for thermal resistance between the absorber and glazing, as well as between the absorber and back wall.

Similar to the absorber, the thermal resistance through the thin glazing is minute, consequently it is ignored, and the glazing is considered to be locally isothermal. The heat that is transmitted into the glazing (at some intermediate temperature between the collector interior and ambient environment) must be lost from the glazing to the environment. These external radiation and convection resistances are:

$$\frac{1}{R_{c-a}} = \frac{1}{R_{conv\,c-a}} + \frac{1}{R_{rad,c-a}} = h_{c-a} + 4\sigma\varepsilon_c T_{avg}^3$$

Rearranging:

$$R_{c-a} = \frac{1}{h_{c-a} + 4\sigma\varepsilon T_{avg}^3}$$ Equation 5-7

Where:

R_{c-a} = Thermal resistance network of the cover to ambient (^oC-m^2/W)

$R_{conv\ c-a}$ = Thermal resistance due to convection between the cover to ambient (^oC-m^2/W)

$R_{rad\ c-a}$ = Thermal resistance due to radiation between the cover to ambient (^oC-m^2/W)

h_{c-a} = convection heat transfer coefficient between the cover to ambient (^oC-m^2/W)

Since R_{c-a} and R_{p-c} are in series, these resistances can simply be added, which gives:

$$R_T = 1/U_T = R_{c-a} + R_{p-c} = \frac{1}{h_{c,c-a} + 4\sigma\varepsilon_c T_{av\ c-a}^3} + \frac{1}{h_c + \frac{4\sigma T_{Ave}^3}{\frac{1}{\varepsilon_p} + \frac{1}{\varepsilon_c} - 1}}$$ Equation 5-8

Where:

U_T = Overall heat loss coefficient for the top of the collector (from plate to ambient) (W/m^2-^oC)

R_T = Thermal resistance network of the top of the collector (from plate to ambient) (^oC-m^2/W)

In a similar manner, the back loss coefficient is developed. The resistance network is identical with the exception being the heat escaping through the back must go through two sheets of 3/8” of plywood and 3.5” of fiberglass insulation; the latter of

which predominates the thermal resistance. The back loss thermal resistance can be described in Equation 5-9.

$$R_B = 1/U_B = \frac{1}{h_c + \frac{4\sigma T_{Ave}^3}{\frac{1}{\varepsilon_p} + \frac{1}{\varepsilon_b} - 1}} + \frac{L_{Ins}}{K_{Ins}} + \frac{L_{pw}}{K_{pw}}$$ Equation 5-9

Where:

U_B = Overall heat loss coefficient for the bottom of the collector (from plate to collector back) (W/m^2-^oC)

R_B = Thermal resistance network of the top of the collector (from plate to collector back) (^oC-m^2/W)

L_{Ins} and L_{pw} = Length of insulation and plywood respectively (m)

K_{Ins} and K_{pw} = Thermal conductivity of insulation and plywood respectively (W/m-^oC)

There is a third heat loss mechanism from the collector, namely side losses. However, because, the side area is modest relative to the collector face area, and the side is insulated, a quick side calculation shows it to be insignificant.

Finally, employing Equation 5-8 and Equation 5-9 we get the collector loss coefficient (U_L); where $U_L = U_T + U_B$.

It is necessary to evaluate the heat transfer coefficient of the air flowing over surfaces inside the collector, h_c. Out of several possibilities, the Second Petukhof

Equation is recommended as the most accurate formulation for the Nusselt Number and is depicted in Equation 5-10 below (Duffie & Beckman, 1980), (Cengel & Turner, 2001).

$$Nu = \frac{h_c * D_H}{k_{air}} = \frac{\mathbf{Re} * \mathbf{Pr}(\frac{f}{8})}{1.07 + 12.7\sqrt{\frac{f}{8}}(Pr^{\frac{2}{3}} - 1)}$$ Equation 5-10

Where:

Nu = Nessult Number (Unitless)

h_c = convection coefficient (W/m^2-^{o}C)

D_H = Hydrolic Diameter of collector ducts (m)

k_{air} = Thermal conductivity of air (W/m-^{o}C)

Re = Reynolds Number (Unitless)

Pr = Prandelt Number (0.72 for air)

f = Friction factor for the collector (assumed to be 0.04 based on the Moody diagram)

The Reynold's Number for non-circular tubes is based upon the hydraulic diameter, as is the Nusselt Number.

$$D_H = \frac{4A}{P} = 4 * \frac{0.116\ m^2}{2(2.28+.05)\,m} = 0.1m$$ Equation 5-11

The Goldade Collector flow channel resembles flow between two infinite plates of separation of 2" (= 0.05 m).

The blower delivers 500 cfm (= 0.24 m^3/s) through a channel flow area A_{gap} = (7.5 ft)(.166 ft) = 1.245 ft^2. (= 0.115 m^2) Therefore the average velocity can be described in Equation 5-12.

$$V = \frac{Q}{A_{gap}} = \frac{0.118\,m^3/s}{0.05m * 2.29m} = 1.03\ m/s \qquad \text{Equation 5-12}$$

For an average interior collector air temperature of 100°F (38°C) the air kinematic viscosity is v_{air} =1.67*10^{-5} m^2/sec and the air thermal conductivity k_{air} = 0.0268 W/m^2-°C. Neither v_{air} nor k_{air} are strong functions of temperature, so they will remain constant regardless of assumed temperature (Cengel & Turner, 2001). Then Reynolds number is:

$$Re = (Renoylds\ Number) = \frac{\frac{1.03\,m}{s} * 0.1m}{1.67 * 10^{-5}\,m^2/s} = 6155 \qquad \text{Equation 5-13}$$

This Reynolds number is well within the turbulent flow region. The channel in which the air passes in the collector is relatively smooth, and a friction flow factor (f) is assumed to have a relative roughness of 0.005. Then from a Moody diagram one reads f ≈ 0.04 based on the Reynolds Number and the assumed roughness of 0.005 (Cengel & Turner, 2001). With these inputs Equation 5-10 yields:

$$Nu = \frac{h_c * Dh}{k} = \frac{6155 * 0.71(\frac{0.04}{s})}{1.07 + 12.7\sqrt{0.04/8}(0.71^{\frac{2}{3}} - 1)} = \frac{21.85}{0.8866} = 24.645$$

$$h_c = Nu * \frac{k}{Dh} = 24.645 * \frac{0.0268}{0.1} = 6.60 \frac{W}{m^2 - °C}$$ Equation 5-14

Determining a value for the convection heat transfer coefficient is a major step toward facilitating the use of Equation 5-8 and Equation 5-9.

In Equation 5-9 the expressions for linearized radiative thermal conductance take the same form as in Equation 5-8. At long wavelength, generally the emissivities can be approximated to be 0.9 ($\varepsilon \approx 0.9$). If the average temperature between the absorber and back wall (or glazing cover) is T_{Ave} = 135°F (57°C) = 580°R (338°K), then the radiative heat transfer coefficient (h_r) can be found.

$$h_r = \frac{4 * 5.67 * 10^{-8} * (57 + 273)^3}{\frac{1}{.9} + \frac{1}{.9} - 1} = 6.66 \frac{W}{m^2 - °C}$$ Equation 5-15

Table 5-2: h_r versus T_{Ave} (h_r = BTU/hr-ft^2-°F or/ W/m^2-°C)

T_{Ave} °F/°C	90/32	100/38	110/43	120/49	130/54.4
h_r	0.93/5.3	0.98/5.6	1.04/5.9	1.09/6.2	1.14/6.52

Table 5-2 indicates that for the T_{Ave} range of interest; as is shown, h_r is a weak function of temperature. Therefore, if a representative value of h_r is selected, the final value of U_L will not be heavily impacted.

The average temperature between the glazing and ambient air will be somewhat less than between surfaces inside the collector. A reasonable $T_{av\ c\text{-}a}$ = 100°F = 38°C. In Equation 5-7 the radiation heat loss from the cover glazing to atmosphere is given as:

$$h_r - glazing\ and\ amb = \quad 4 \in \sigma T_{Ave}^3 = 4 * 0.9 * 5.67 * 10^{-8} * (38 + 273)^3 = 6.02 \frac{W}{m^2 - °C}$$

Equation 5-16

An expression for convection (only) loss to the ambient from a glazing cover in terms of wind velocity is $h_{c\text{-}a}$ = 0.5 + 0.16V where h≈ BTU/hr-ft^2-°F and V ≈ ft/sec [Recall 60 mph = 88 fps] (Duffie & Beckman, 1980). At a wind speed of 5 mph = 7.33 fps; $\underline{h_{c\text{-}a} = 1.67\ BTU/hr\text{-}ft^2\text{-}°F}$, = 9.16W/m^2-^{o}C. Then using Equation 5-8, the top loss coefficient is readily calculated. At this specified wind velocity. $R_{Top} = 1/U_T = 1/[9.16+6.02] + 1/(6.58+6.02) = 0.142\ m^2\text{-}^oC/W$ $R_{Top} = 0.142\ m^2\text{-}^oC/W$ >>> $\underline{U_T = 1/R_{Top} = 7.27\ W/m^2\text{-}°C}$

The thermal resistance of 3½" fiberglass batt insulation is $\underline{L_{Insul}/k_{insul} = 11\ hr\text{-}ft^2\text{-}°F}$. The thermal resistance of two 3/8" thick plywood sections is $\underline{L_{pw}/k_{pw} = 0.94\ hr\text{-}ft^2\text{-}°F}$. Similarly, using equation the equation below (Cengel & Turner, 2001).

$$R_B = 1/U_B = \underset{\text{Abs-to-back}}{0.63} + \underset{\text{Insul}}{11} + \underset{\text{Plywood}}{0.94} = 12.57 \quad >>> \quad U_B = 0.08 \text{ BTU/hr-ft}^2\text{-°F}$$

$$U_B = 0.45 \text{ W/m}^2\text{-°C} \qquad \text{Equation 5-17}$$

Clearly the insulation dominates the back loss coefficient, which illustrates the importance of having adequate insulation in stand-alone collector design. Finally, the overall Heat Loss Coefficient $U_L = U_T + U_B$ is $U_L =$ 7.78W/m^2-°C.

Determining F' & F_R: A 2013 analytical study for parallel pass single glazing air collectors (such as the Goldade Collector) offers the following correlations to determine the efficiency factor (F') (Hernandez & Quinonez, 2013).

$$F' = \frac{h_{c,p-c}\Sigma_1\Sigma_2 + h_{r,p-c}h_{c,p-c}\Sigma_1}{\Sigma_3} + \frac{h_{c,p-b}\Sigma_1\Sigma_2 + h_{r,p-b}h_{c,p-b}\Sigma_1}{\Sigma_3} \qquad \text{Equation 5-18}$$

Where:

$$\Sigma_1 = U_t + h_{c,p-c} + h_{r,p-c}$$

$$\Sigma_2 = U_b + h_{c,p-b} + h_{r,p-b}$$

$$\Sigma_3 = \left(h_{c,p-c} + h_{r,p-c}\right)\Sigma_1\Sigma_2 + h_{r,p-c}(U_t + h_{c,p-c})\Sigma_1 + h_{r,p-b}(U_b + h_{c,p-b})\Sigma_1$$

Solving the above equations with the heat transfer coefficients determined in the above analyses yields an F' of 0.86.

The equation for F_R (The Heat Removal Factor) is given for most solar air heaters, and specifically for the Goldade solar collector, by (Duffie & Beckman, 1980)

$$F_R = \frac{mC_p}{U_L A_c}\left[1 - e^{\frac{-F' A_c U_L}{mC_p}}\right] \qquad \text{Equation 5-19}$$

The density will be that of the ambient temperature at an altitude of 4400 ft, which is 0.937 kg/m^3. The mass flow rate (m) = ρ*Q = 0.221 kg/s. Combining these values with the overall heat loss coefficient (7.49 W/m^2-°C), the area of the collector (11.89 m^2), and the specific heat of air (Cp) = 1.006 kJ/(kg-^{o}K) yields F_R = 0.728 as is shown.

$$F_R = \frac{0.221kg/s * 1006\ j/(kg-°K)}{7.49\frac{W}{m^2-°K} * 11.89\ m^2}\left[1 - e^{\frac{7.49\frac{W}{m^2-°K} * 11.89\ m^2 * 0.86}{0.221kg/s * 1006\ j/(kg-°K)}}\right] = 0.728 \qquad \text{Equation 5-20}$$

Finally using Equation 5-2 and Equation 5-3, the x and y intercepts are found to be 0.099 and 0.574 respectively, and the following graph is developed as Figure 5-2.

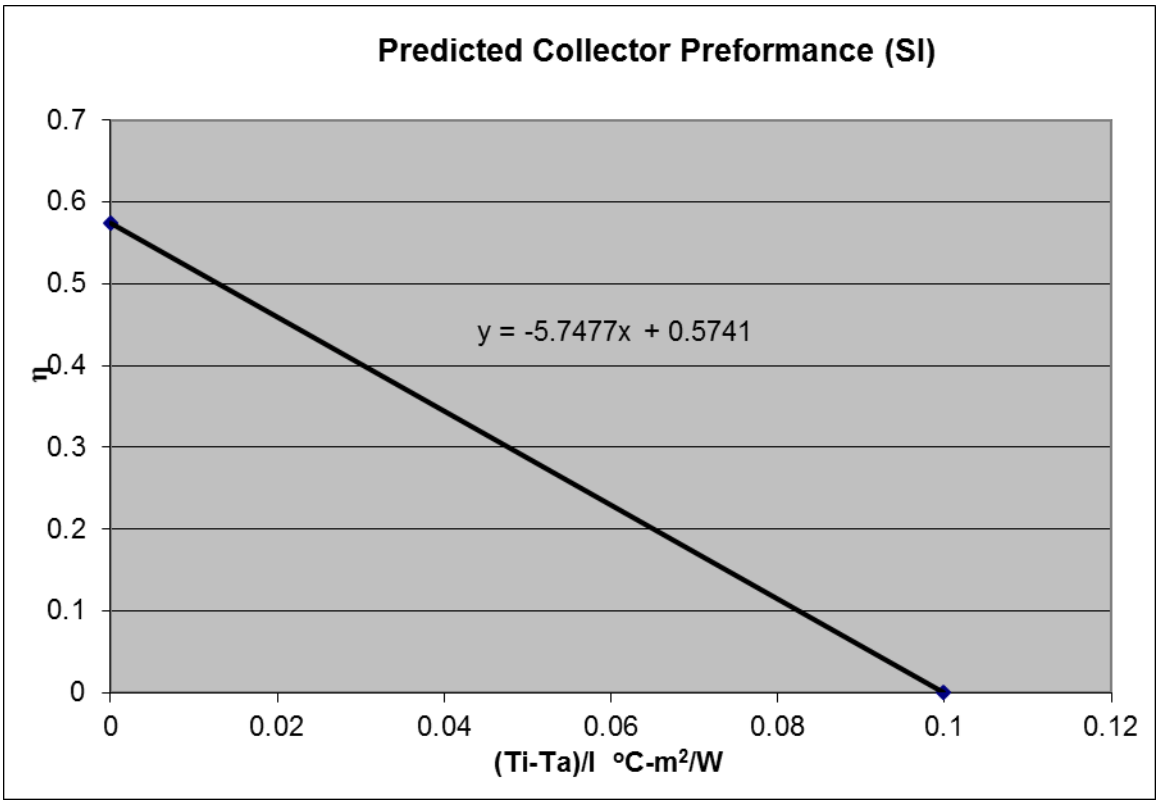

Figure 5-2: Theoretical Performance Curve for the Goldade Collector.

Technical Evaluation using the MSEL

Tests were conducted November 20th through November 23rd, 2015 to test the performance of the Goldade collector in winter time conditions. It should be noted that the procedure for collecting data outlined in Chapter 4 was closely followed with the exception of the use of a butterfly valve, as adequate funding could not be obtained. To acquire the differing air intake temperatures the outlet duct was ducted to the intake is simulate the stagnation condition ($T_{in} = T_{out}$). To simulate ambient conditions, the outlet duct was simply removed from the vicinity of the inlet duct, as to ensure no heated air

would enter the system ($T_{in} = T_{amb}$). To simulate the intermediate points the outlet duct partially enclosed the inlet duct. This partial enclosure allowed for both ambient and heated air to be drawn into the system. See Figure 5-3 through Figure 5-5 for the testing conditions.

Figure 5-3: $T_{in} = T_{amb}$

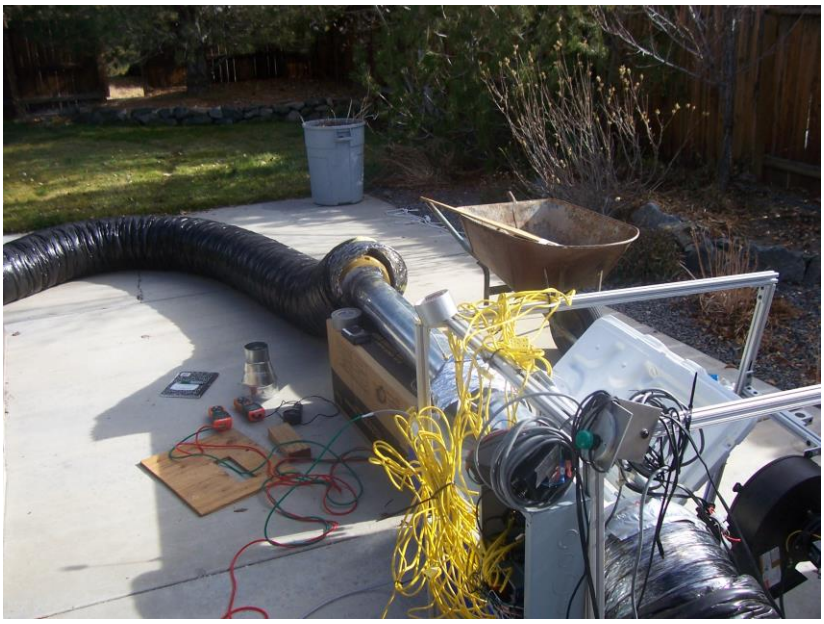

Figure 5-4: $T_{in} = T_{out}$

Figure 5-5: Intermediate Point

Per normal procedure, the test data shown in Figure 5-6 were corrected with Figure 3-3 and Equation 5-1 to apply the incident angle modifier. The theoretical prediction shown in Figure 5-8 was found with the methods described in the previous section except modified for the lower flow rate of the MSEL pumps (measured to be ~ 320 cfm).

Figure 5-6 reveals that the empirical performance curve developed from hand collected data compares favorably to the theoretical performance curve. This demonstrates that hand collection of data is a viable method to conduct field tests on SBACs. It should be noted that the stagnation conditions could not be achieved. The most likely reason for this is there was leakage when the inlet and outlet ducts were attached for the tests. Because of this ambient air was most likely being drawn into the system. So, the x- abscissa data points were not obtained in Figure 5-6 during testing.

In Table 5-3 the experimental and theoretically-derived collector coefficients are compared. With the exception of the overall heat loss (U_L) all of the experimentally predicted performance parameters were accurately predicted. One would expect the collector to have a higher heat loss than what is theoretically predicted from a 2 year old collector exposed to the elements that was constructed by amateurs than what would be predicted in calculations. The most likely source of error would be that of leakage which was not accounted for in the theoretical calculations.

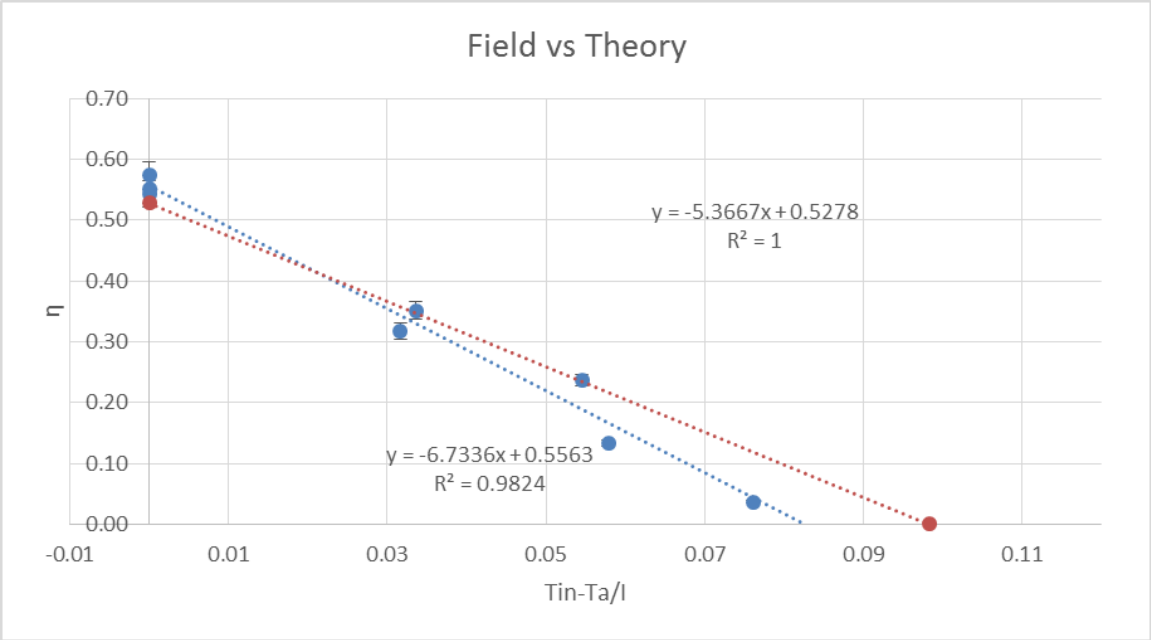

Figure 5-6: Field vs Theoretical Curves of Goldade House Red Data = Theoretical Estimate; Blue Data = Field Data from November 20th – 23rd

Table 5-3: Comparing Theoretical to Field Test Parameter Values for the Goldade Collector

$\tau^*\alpha = (0.86)(0.9) = 0.774$

Parameter	U_L W/m^2-°C	F'	F_R	X ~ $\tau\alpha/U_L$	Y ~ $\tau\alpha F_R$
Theory	7.87	0.89	0.68	0.10	0.53
Field Test	9.37	0.89	0.72	0.083	0.54

Chapter 6. System Description and Cost

Figure 6-1 shows the Goldade household designed and constructed a parallel pass single glazed SBAC; it was built in the summer of 2013. Figure 6-2 through Figure 6-5 were drawn to facilitate the discussion and indicate dimensions of the collector and the system configuration relative to the house. The collector's exterior dimensions are 8' x 16'3" with an aperture area of 15'4" x 7'2" built at a 60^{o} angle from horizontal. The unit faces due south. The glazing is 0.060" thick SUN-LITE® glazing material; the absorber is double layered 30 millimeter black felt. The felt is placed in the center of the 4" gap between the glazing and the back of the collector as to create two 2.0" gaps for the air to pass above below the absorber. The back of the collector consists of two pieces of 3/8" plywood, in-between the plywood layers is 3.5" of fiberglass insulation. The exterior frame of the collector consists 8' wooden 2" x 4" with rigid 1" Styrofoam insulation placed in the interior. The internal structure is supported by slotted wooden 2"x4"s spaced every 2' to allow for a stable structure for the glazing and felt absorber. The slotted 2"x4"s consists of five 5" pieces spaced approximately 1' apart on the vertical of the collector to facilitate air flow (see Figure 6-3). The base is supported by 10 custom made 2"x 4" wooden pieces that are bolted to a 1.0' x 17' concrete slab; the top of the collector is supported by the wall of the house.

The intake air is obtained from the crawl space of the house and the air exit is located in the kitchen (see Figure 6-4 and Figure 6-5), powered by a 10" RS10 HO 283

Watt Can Fan blower which is rated at 761 CFM at no load (Can-Filters, 2007). The air travels through approximately 20’ of 12” insulated flex duct before it enters the collector, and a further 35’ of 12” flex duct to the outtake. The flow rate of the system was measured during testing to be approximately 500 CFM. According to the manufacturer this would equate to approximately 1" of H_2O head loss throughout the system when it is in operation (see Figure 6-6).

Figure 6-1 Goldade SBAC

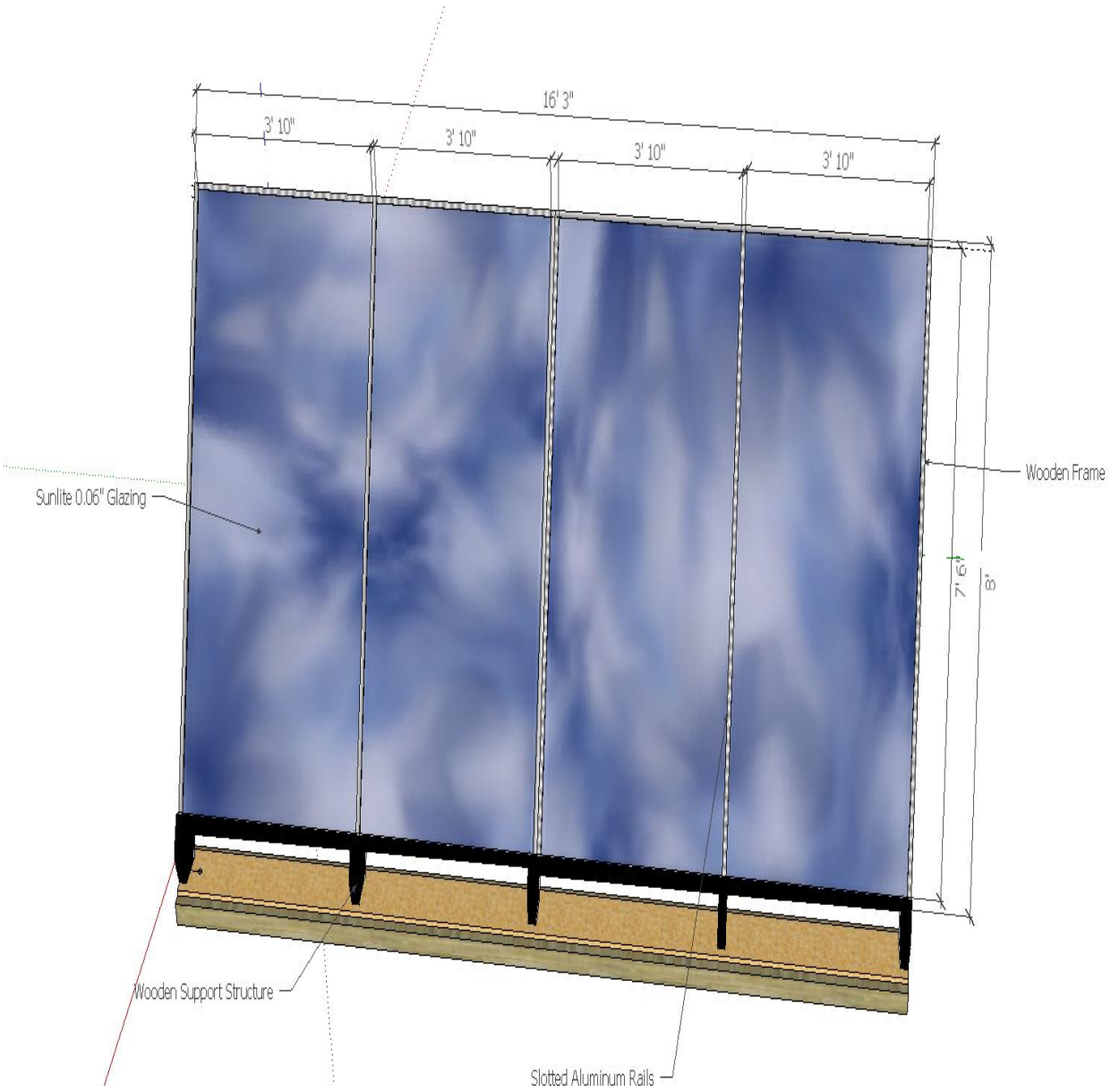

Figure 6-2 Front View of Goldade SBAC Sketch up

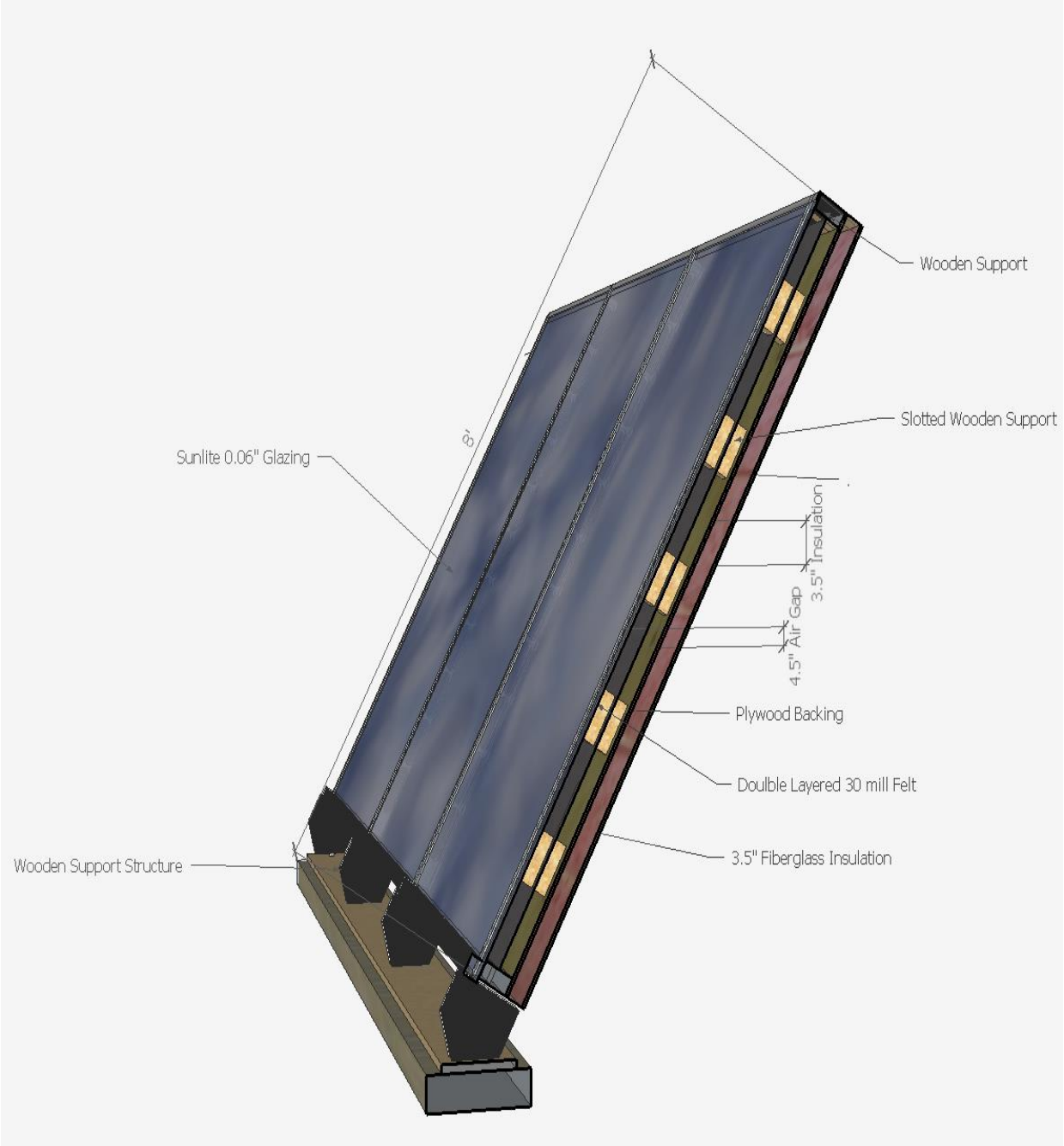

Figure 6-3: Side View Cut Away of Goldade SBAC

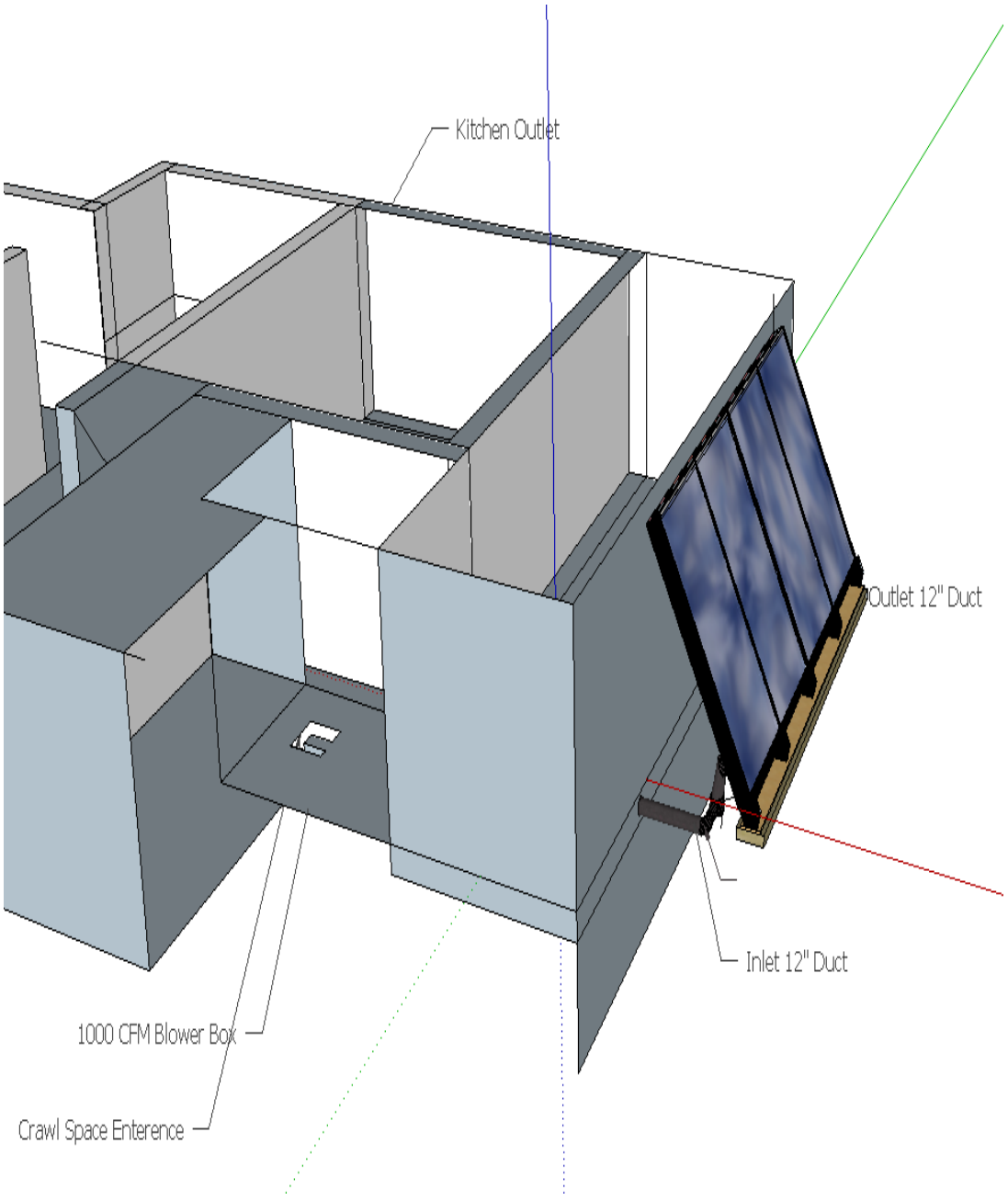

Figure 6-4: SBAC and House

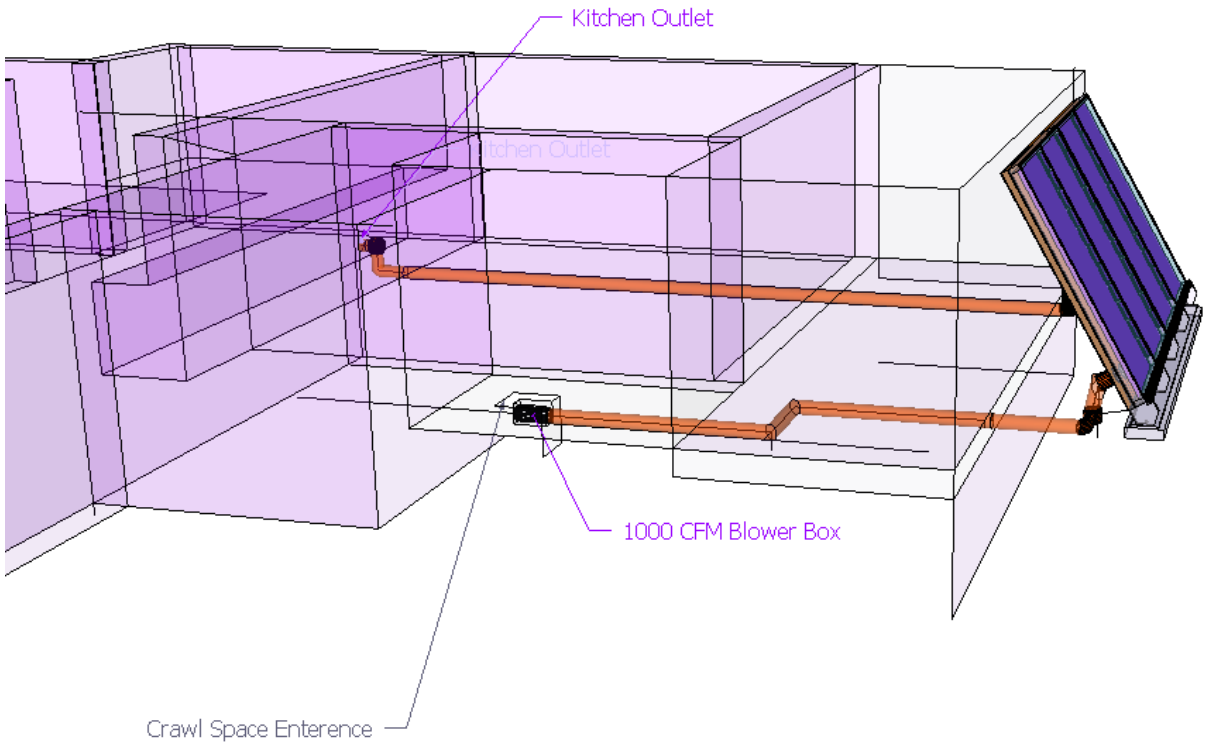

Figure 6-5: Duct Configuration

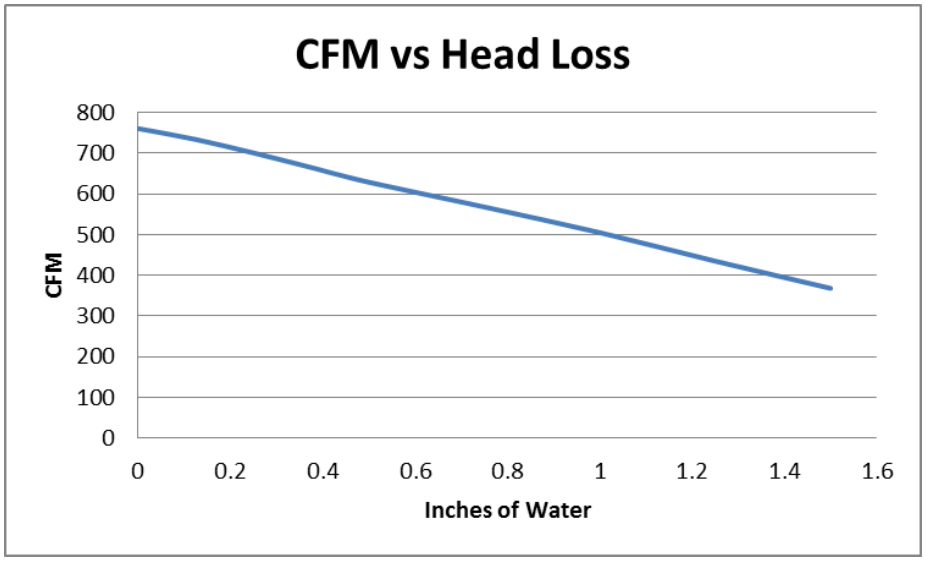

Figure 6-6: RS10 Blower Curve (Can-Filters, 2007)

The total cost of the system is summarized in Table 6-1; nearly all materials were obtained from a local home improvement store, with the only exceptions being the glazing material and the blower. The glazing was obtained from Solar Components Corporation located in New Hampshire, and the blower was purchased from EBay. The pricing was obtained from the parent companies websites (Solar Components Corporation, 2015) & (Home-Depot, 2015). The total time required to construct the system was approximately 40 man hours, with an assumed rate of $ 20/hour the total estimated labor was obtained.

Table 6-1 Goldade SBAC Estimated Costs

Goldade SBAC Costs				
Material	Cost/unit		Ammount	Total Cost
Blower	$ 200.00	unit	1	$ 200.00
Plywood	$ 0.42	ft^2	256	$ 107.52
2x4's	$ 0.35	ft	78	$ 27.30
Inslation	$ 0.52	ft^2	128	$ 66.56
Ground Cloth	$ 0.25	ft^2	256	$ 64.00
Glazing	$ 4.00	ft^2	128	$ 512.00
Flext Duct	$ 2.00	ft	60	$ 120.00
Concrete	$ 5.40	bag	13	$ 70.20
Miscellaneous	N/a		N/a	$ 200.00
Labor	$ 20.00	hr	40	$ 800.00
			Total	**$ 2,167.58**

The collector was constructed during the summer of 2013, and has been in operation for the last 2 years. During the heating months (October through April) the collector is uncovered and the system is allowed to operate. During the remaining

months the collector is covered with an opaque tarp to prevent the collector from overheating and destroying the felt absorber. Originally the collector was designed to be 8' by 24' and the cover material was tempered glass. However, it was quickly determined that the glass was far too difficult to work with due to the house-hold's limited construction skills. Furthermore, at this size and configuration the collector ran too hot (outtake temperatures were in excess of 150 ^{o}F). At these high temperatures the felt absorber would melt when uncovered. Due to these issues, the glass cover was switched out for SUN-LITE® glazing material, and the collector size was decreased to 8' by 16'. After these changes were implemented the collector was constructed in a weekend's time, and the collector ran at acceptable temperatures, with typical outlet temperatures ranging from 110 ^{o}F to 135 ^{o}F depending on the ambient weather conditions.

After the design changes were enabled, in the 2 years of operation, there have been no major maintenance problems. Furthermore, provided the weather is conducive to strong insolation, the collector is nearly continuously in operation. This is demonstrated by a total time of 1617 hours recorded by a timer set to turn on when the blower is in operation. The blower is programmed to start when a thermocouple in the collector detects temperatures in excess of 100^{o}F. Typically, the collector will turn on around 10:00 am and will operate continuously until 3 to 4 pm, provided the weather is conducive to solar heating. During days of extreme cold (temperatures below freezing)

the collector has been observed to turn on as late as 11:30 and turn off as early as 2:30 during days of strong insolation. However, this has been seldom observed.

Overall the house-hold is extremely satisfied with the collector. Due to the blower's location and non-intrusive design, the only noise generated is a gentle hum, which can only be heard if one is near the crawl space in which it is located. Typically the only indication that the collector is in operation is the sound of air flowing through the exit vent located in the kitchen. As a result of the outlet duct's location (see Figure 6-4 and Figure 6-5) being centrally located to the main living area, the heat is delivered to the rooms that are typically occupied most often (the kitchen, living room and dining room). This not only allows for the conventional heating system to be utilized for less time during the day, but it is also not uncommon for the main living area to be heated in excess of the typical temperatures the house is traditionally kept at (65 ^{o}F when occupied 55 ^{o}F when unoccupied). This allows for a greater comfort level than what is routinely enjoyed during the winter months.

The only complaints of the systems are that there is no storage, so the heat generated is not typically enjoyed during the work week (however the house is noticeably much warmer upon entering the house when it is unoccupied). There is no practical use for the collector during non-winter months, and during early usage (the first few months) the collector had an unpleasant odor at the outtake during operation. However, currently, the only scent generated is a slight lumber smell, which is non-intrusive and even slightly pleasant. Due to the overall satisfaction of the collector and

low cost of the system when compared to comparable commercial systems, it is not uncommon for the house hold to recommend a similar system to others if they are interested is solar heating.

Chapter 7. Economic Performance of the Goldade Solar System

There are three steps to conducting a solar system economic analysis. First it is necessary to know the cost of the system. Second, the annual energy provided by the system must be estimated, after which the value of this heat is calculated from defrayed energy purchases. Finally the payback period can be estimated by comparing the value of the useful solar gain to the (after-tax) money saved from conventional heat purchase.

The cost of the Goldade System is known from Chapter 6 in two modes. The material cost of the homeowner built system was found in Table 6-1 to be $1308, and since Family Goldade provided the (free homeowner) labor that is the total system cost. However, if the labor were hired at conventional rates, 40 hours at $20/hr, then Table 6-1 gives the system cost at $2108.

f-Chart Estimate of the Goldade System

There are various ways to estimate the annual useful heat production by a solar heating system. A standard and straight forward technique is the f-Chart Method. The f-Chart Estimate provides annual useful outputs based on correlations of numerical simulations of solar thermal systems, which are correlated in terms of relatively easily calculated dimensionless variables. The result of these simulations is a monthly fraction (f) of the heating load that can be supplied by a collector of given size and performance parameters for a given location (Duffie & Beckman, 1980). For this thesis it estimates the total useful heat gathered throughout a winter season for the Goldade system,

facilitating calculating heating money saved and thus an economic payback period. This chapter will summarize the applicable equations and present a final annual heating fraction, and hence the total useful annual heat contribution that the solar heating system provides at the Goldade residence.

The great utility of the f-Chart method is its simplicity. Two dimensionless parameters, X and Y are calculated from basic data, and then a function "f" is calculated from these values. "f" is defined as the fraction of heating demand for the considered month delivered by the solar heating system.

$$X = F_R U_L * \frac{F'_R}{F_R}\left(T_{Ref} - T_{a,avg}\right)\Delta t * \frac{A_c}{L} \qquad \text{Equation 7-1}$$

$\underline{X_C/X} = (21.7/10)^{0.28} = \underline{1.24}$ for the Goldade System Equation 7-2

$$Y = F_R \tau\alpha_n * \frac{F'_R}{F_R} * \frac{\tau\alpha_{avg}}{\tau\alpha_n} * H_T N * \frac{A_c}{L} \qquad \text{Equation 7-3}$$

$$f = 1.040Y - 0.065X_c - 0.159Y^2 + 0.00187{X_c}^2 - 0.0095Y^3 \qquad \text{Equation 7-4}$$

Where:

Δt= The time in a month in seconds (seconds/month)

H_T = Radiation striking a tilted surface (60° for Goldade Collector) for a given location and month J/m^2-month

L = Estimated space heating load of the house during a month (J/month)

N = Number of days for a given month

$T_{a,avg}$ = Average ambient temperature for a given month for a location

T_{ref} = 100 ^{o}C

$\frac{F'_R}{F_R}$ = Heat transfer to medium (= 1 for air collectors)

$\frac{\tau\alpha_{avg}}{\tau\alpha_n}$ = average τα product for a given month this = 0.96 for most collector configurations (Duffie & Beckman, 1980)

Xc = Correction factor for differing flow rates (see below)

Y & X = Analytically-derived dimensionless parameters to determine the fractional heating load

f = Fractional heating load to be supplied by solar collector

Each parameter in Equation 7-1 through Equation 7-3 will be discussed and/or evaluated, so that f can be evaluated for each month by Equation 7-4. Then the normalized monthly f's can be summed to determine the annual f.

Equation 7-1 is based on a collector air flowrate per unit collector area of 10 liter/sec-m^2 = 2 cfm/ft^2, so if the flowrate is other than 10 l/s-m^2 then X needs to be corrected to X_C by Equation 7-2. Then X_C will be used in Equation 7-4 instead of X. This correction is necessary because higher flowrate is associated with higher efficiency, more heat at lower temperature and thus lower losses. Since the Goldade system uses a 500 cfm flowrate blower for a 115 ft^2 collector, the air flowrate per unit collector area is 500/115 = 4.35 cfm/ft^2 = 21.7 l/sec-m^2. Therefore for this analysis Equation 7-2 yields

$\underline{X_C/X}$ = $[21.7/10]^{0.28}$ = $\underline{1.24}$. This value shown in Equation 7-2 and will be used throughout the calculation.

For the Goldade collector $\underline{F'_R/F_R = 1}$, because there are no thermal losses since the heated air is delivered directly to the house (Duffie & Beckman, 1980). The tau-alpha (τ-α) correction for non-normal incident insolation, is discussed by Klein, who also developed the f-Chart (Klein, 1979). Although close approximations to the τ-α correction could be developed for each month, it is recommend to utilize an average value of $\frac{\tau\alpha_{avg}}{\tau\alpha_n}$ = 0.96 for south oriented collectors tilted at 60° from horizontal around 40° latitude (Klein, 1979). This matches the Goldade collector, and this recommendation is adopted here.

The monthly winter house heating load L appears in both Equation 7-1 and Equation 7-3. L is assessed by first estimating the overall heat loss coefficient for the house, U_L, then multiplying U_L by the number of degree days. A degree day, by definition, is the total number of days the average temperature is above or below a reference temperature. For most winter calculations the reference temperature is 16 °F or 18.3 °C. However, as will be described later, the reference temperature was modified to 58 °F or 14.4 °C. This was done to reflect the actual heating demand of the house. U_L consists of several components including heat loss through walls, windows, ceiling, floor, and infiltration. There are many reliable sources for estimating each component. ASHRAE is the standard source for this technology, and provides convenient

authoritative sources for coefficients and information (ASHRAE Handbook of Fundamentals, 2001).

The total square footage of the house is 2200 ft^2, with a perimeter of 296 ft; values of window area of 10% of total area, an average wall height of 8 ft. Then with U_i parameters taken from standard values Table 7-1 indicates the component heat loss coefficient for the Goldade house is (U*A) House = 251 Watt/°C (ASHRAE Handbook of Fundamentals, 2001).

Table 7-1: Heat loss of Goldade House

Component	Area (A) ft^2/m^2	U_i W/m^2-°C	$(UA)_i$ W/°C
Walls	2131 / 198	0.45	89.1
Windows	237 / 22	3.2	70.4
Ceiling	2200 / 205	0.28	57.3
Floor	2200 / 205	0.17	34.6

$(U*A)_{House} = \Sigma(U*A)_I =$ 251 Watt/°C

The final major component of heat loss is due to infiltration (Q_{inf}). With an estimated volume of 17600 ft^3, air change rate of 0.75 air changes/hr (ACH), and appropriate values for the air density and temperatures, the house load due to infiltration is:

$Q_{Infil} = \rho V_H(ACH) c_p (65 – T_{Amb})=(0.065 lb/ft^3)(17{,}600 ft^3)(0.75)(0.24 BTU/lb\text{-}°F)(\Delta T)$

$\underline{Q_{Infil}} = (251 BTU/hr\text{-}°F) (65°F – T_{Amb}) = \underline{(108.6 Watt/°C) (18.3°C - T_{Amb})}$ Equation 7-5

Since the total house heat load is due to both house losses and infiltration, we can write Equation 7-6.

$Q_{Total} = (UA)_{Tot}(18.3\text{-}T_{Amb}) = (251 W/°C)((18.3\text{-}T_{Amb}) + (108.6)(18.3\text{-}T_{Amb})$ Equation 7-6

Or: $\underline{(UA)_{Tot} = 360 Watt/°C}$,

This is the total heat loss parameter for the Goldade house, and allows estimate of the heating load for each month.

As was stated above, standard calculation techniques are based on a house interior temperature of 65°F = 18.3°C. However, Family Goldade is habituated in winter to set the thermostat to 58°F = 14.4°C at night and when the house is empty. Normally the household consists only of Mr. and Mrs. Goldade, who set the thermostat at 58°F when they retire at 11 pm. Monday through Friday when they get up and prepare for work, they do not turn up the thermostat. When one of them gets home around 4 pm he/she sets the thermostat to 65°F, where it stays until 11 pm. On the weekends the thermostat is set at 65°F from 7 am to 11 pm, after which it is set to 58°F. The schedule is summarized:

Thermostat set at 58°F:

M >> F 11 pm ⍰4 pm >> (17 hr)(5 days/week) = 85 hr

S & S 11 pm ⍰7 am >> (8 hr)(2 days/week) = <u>16 hr</u>

Normal total = 101 ≅ 100 hr/week at 58°F

So the average thermostat setting (house interior temperature) is: T_{in} = [(100 hr)(58°F) + (68 hr)(65°F)]/168 hr >>> T_{in} = 60.8°F = 16°C. This value will be used in load calculations.

The data necessary to exercise Equation 7-1 and Equation 7-3 are shown in Table 7-2 (Duffie & Beckman, 1980). These data constitute the required information to determine the solar insolation in the Reno area over the pertinent months.

Table 7-2: Meteorological Data For Reno, NV Latitude 39.5°

	Oct	Nov	Dec	Jan	Feb	Mar	Apr
H_H J	1.62E+07	1.04E+07	8.01E+06	9.09E+06	1.31E+07	1.87E+07	2.45E+07
K_T	.71	.62	.57	.59	.63	.71	.73
T_{Amb} °C	10	4	1	0	3	5	8
DD °C/m	262	417	550	572	436	428	309

H_H Monthly average daily radiation on a horizontal surface ~ J/m^2
K_T Monthly average clearness index (Unitless)
T_{Amb} 24-hour monthly average ambient temperature ~ °C
DD Average number of degree days in the month to base temperature 18.3°C (65°F)

Monthly Heating Load, L:

With Equation 7-6 and the meteorological information in Table 7-2 it is possible to calculate the monthly Goldade House winter heating load each month, L, which appears in both Equation 7-1 and Equation 7-3. The calculation is illustrated below for January, and all winter months are summarized in Table 7-3. A sample calculation is provided below:

$L_{Jan} = (UA)_{Tot} (T_{in}-T_{Amb})(744 \text{ hr/mo})$

$= (360 \text{ Watt/°C})(16°C-0°C)(744 \text{ hr/Jan})(3600 J/W\text{-hr})$

$L_{Jan} = 15.4 \times 10^9 \text{ J} = 15.4 \text{ GJ/Jan} \quad [4285 \text{ kWh/Jan}]$

Table 7-3: Monthly Heating Load for Goldade House (L ~ Joules)

	Oct	Nov	Dec	Jan	Feb	Mar	Apr
T_{Amb} °C	10	4	1	0	3	5	8
L_i J	5.79E+09	1.12E+10	1.45E+10	1.54E+10	1.13E+10	1.06E+10	7.46E+09

The total annual heating load is ΣL_i = 74.0 GJ = 20,600 kWh.

Average Daily Insolation on Collector for each month, H_T:

For each month H_H, the average daily insolation incident on a horizontal surface, is read from Table 7-2. Now this H_H must be translated to incident solar gain on the Goldade collector (H_T), which faces due south (Azimuth $\gamma = 0$) and is inclined $\beta = 60°$ from horizontal. The declination changes with season as the sun appears to move. For

the middle of each month the declination (angular distance from the celestial equator, δ) is given in Table 7-4 (Duffie & Beckman, 1980).

The relationship relating H_T to other parameters has been shown to be Equation 7-7. The first term on the right side corrects insolation on a horizontal surface to a tilted surface through the geometric factor R_b. The second term accounts for the diffuse atmospheric radiation contribution. The third term allows for reflected ground radiation, which can be appreciable on a high-tilt collector if snow is on the ground. Normally the ground reflectance ρ = 0.2, but when snow is on the ground the third term augmentation can be appreciable. To be conservative (tending toward lower insolation estimates) in this study, ρ = 0.2.

$$H_T = H_H R_b + H_d * \frac{1+\cos(\beta)}{2} + H_H \rho \frac{1-\cos\beta}{2}$$ (Collector slope β = 60°) Equation 7-7

Where:

ρ = Reflectance of ground around collector (Unitless)

H_d = Monthly daily average diffuse radiation striking a horizontal surface for a given location and time (J/m^2)

H_H = Monthly daily average radiation striking a horizontal surface for a given location and time (J/m^2)

H_T = Monthly daily average radiation striking a tilted surface (60^o for Goldade Collector) for a given location and time (J/m^2)

R_B = Ratio of beam radiation on a tilted plane to that on a horizontal plane (Unitless)

The diffuse component of solar radiation (H_d) is related to the clearness factor (K_T, given in Table 7-2) by Equation 7-8

$$H_d = \left(1.391 - 3.56 * K_T + 4.189 * {K_T}^2 - 2.137{K_T}^3\right)H_H \qquad \text{Equation 7-8}$$

H_d is also reported in Table 7-4 as an intermediate calculation step toward H_T. R_b is the ratio of beam radiation on the tilted surface to that on a horizontal surfaced at a considered time. The geometric factor R_b is:

$$R_b = \frac{\cos(\varphi-\beta)\cos(\delta)\sin(\omega)+\omega(\sin(\varphi-\beta)\sin(\delta)}{\cos(\varphi)\sin(\delta)\sin(\omega)+\omega\sin(\varphi)\sin(\delta)} \qquad \text{Equation 7-9}$$

Where:

θ = Angle of incidence between sloped collector and incoming beam radiation

δ = Declination angle

φ = Latitude of the collector

β = Slope of the collector from horizontal

γ = Angle of collector from due south

ω = Hour angle

Fortunately, Duffie and Beckman have evaluated the preceding equation for many conditions and present tables of R_b (for γ = 0°, collector facing due south ~ our considered case!) in their Appendix D. For latitude φ=40° and collector tilt β=60°, the appropriate R_b for each month is listed in Table 7-4.

The process for calculating H_T will be illustrated for January, and results for all months are listed in Table 7-4. H_H = 9.09 GJ from Table 7-2. R_b = 2.51. Employing Equation 7-8 and using K_T = 0.59, H_d = 2.81 MJ. Finally using Equation 7-7 with ρ = 0.2 and β = 60° yields

Direct Diffuse Ground

H_T = 22.82 + 2.11 + 0.45 = 25.38 MJ

Examination of the H_T result shows the direct beam component accounts for about 90% of the total received solar gain on the collector; this result is consistent with expectation. However, the diffuse component cannot be ignored and accounts for about 8.3% of the gain. The ground reflection is less than 2%, although if there were snow on an unobstructed ground this component could be higher.

Table 7-4: Determination of H_T, the Total Average Daily Radiation Incident on the Collector

	Oct	Nov	Dec	Jan	Feb	Mar	Apr
δ °	-9.6°	-18.9°	-23°	-20.9°	-13.0°	-2.4°	+9.4°
H_H J	1.62E+07	1.04E+07	8.01E+06	9.09E+06	1.31E+07	1.87E+07	2.45E+07
R_b	1.68	2.32	2.73	2.51	1.88	1.33	0.91
H_d J	3.41E+06	2.95E+06	2.62E+06	2.82E+06	3.61E+06	3.94E+06	4.74E+06
H_T J	3.1E+07	2.7E+07	2.4E+07	2.5E+07	2.8E+07	2.9E+07	2.7E+07

Determination of solar fraction F and Annual Useful Solar Heat Delivered $Q_s = \Sigma f_i L_i$:

Prior to evaluating Equation 7-1 and Equation 7-3 some other parameters need to be established. $F_R U_L$ (the negative slope of the collector efficiency curve) was determined in Chapter 5 to be $F_R U_L = 5.74$. $F_R \tau\alpha_n$ (the y-intercept of the efficiency curve) was shown to be $F_R \tau\alpha_n = .57$. For the Goldade collector $\frac{F'_R}{F_R} = 1$. With these data X_c and Y and subsequently f_i can be calculated. Subsequent to the f_i calculation, the annual heating fraction provided by solar, F, is calculated. The calculation is summarized in Table 7-5. $F = \Sigma f_i L_i / \Sigma L_i$, where : $\Sigma L_i = 74.9$ GJ (see Table 7-3) The total heat defrayed by the solar system each winter can be found as: $Q_s = \Sigma f_i L_i = 262$ GJ = 248 Therms. (Recall 1 Therm = 10^5 BTU) $Q_s = 248$ Therms is the starting point for the economic analysis.

Table 7-5: Calculations to Determine F and Qs

Source		Oct	Nov	Dec	Jan	Feb	Mar	Apr
Table 7-3	L_i J	5.79E+9	1.12E+10	1.45E+10	1.54E+10	1.13E+10	1.06E+10	7.46E+09
Table 7-4	H_T J	3.1E+7	2.7E+07	2.4E+07	2.5E+07	2.8E+07	2.9E+07	2.7E+07
Eqs 7.1,7.2	X_c	4.05	2.16	1.78	1.69	2.02	2.33	3.11
Eq 9.3	Y	1.12	0.49	0.35	0.35	0.47	0.57	0.74
Eq 9.4	f_i	0.69	0.33	0.23	0.23	0.32	0.39	0.48
	F_iL J	4.02E+9	3.72E+09	3.38E+09	3.62E+09	3.67E+09	4.18E+09	3.60E+09

ΣL_i = 76 GJ = 723 Therms, Total Winter Heating Load for the Goldade House.

$\underline{\Sigma f_i L_i = 262 \text{ GJ} = 248 \text{ Therms, Total Solar Contribution to Winter Load.}}$

Economic Performance of the Goldade System:

Previously it was shown that the solar heating system cost Family Goldade $1308. If they had purchased the labor as well as the materials, it would have cost $2108.

Table 7-5 indicates that 248 Therms are saved each winter. The value of a solar investment will vary between different consumers, depending on their source of purchased backup winter heat. Five heating sources and their Simple Payback Periods (SPP) will be considered here. Fuel costs are current for Reno in 2015.

(1) Natural Gas: Cost = \$1.20/Therm. Assume furnace efficiency $\eta_f = 0.85$. Then the saving per year is Annual Saving (AS):

AS_{NG} = (248 Therm/year)(\$1.2.Therm)/0.85 = \$350.62/year

According to the Goldade house-hold records this saving of \$350 for a winter is a reasonable estimate.

SPP_{NL} = \$1308/\$350/year = 3.7 years
SPP_{Lab} = \$2108/\$350/year = 6.0years

(2) Propane: Cost = \$2.25/gal. There are 0.91 Therm/gal. $\eta_f = 0.85$. Then

AS_{Prop} = (248 Therm/year)(\$2.25/gal)/[(0.91 Therm/gal)(0.85)] = \$722.43/year

(3) Electricity: Cost = \$0.10/kWh and 1 Therm = 29.3 kWh Then

AS_{Elect} = (248 Therm/year)(\$0.10/kW-hr)(29.3 kWh/Therm) = \$727.43/year

(4) Heat Pump: COP = 2.5 on average. Then

AS_{HP} = AS_{Elect}/2.5 = \$291.07/year

(5) Number 2 Fuel Oil: Cost = \$2.25/gal. Heat Content = 1.37 Therm/gal. $\eta_f = 0.85$ Then

AS_{FO} = (248 Therm/year)(\$2.25/gal)/[(1.37 Therm/gal)0.85] = \$480/year

These calculations are summarized in Table 7-6 to facilitate comparisons. The SPP is shown both with No Labor (NL) payments and also paying \$800 for labor. The

SPP is also compared both with no external financial incentives and also with a 30% financial inducement.

Table 7-6: Economic Comparison of Five Backup Heating Fuels in Northern Nevada

Solar heating saves 248 Therms/year
System Cost with no labor pay = $1308. System cost with labor = $2108.

Fuel Source	Unit Cost	Annual Savings	SPP_{NL} No Incentives	SPP_{Labor} No Incentives	SPP_{NL} 30% Incentive	SPP_{Lab} 30% Incentive	kg CO_2/Therm	kg CO_2 Savings/yr
Nat. Gas	$1.20/ Therm	$ 350.62	3.7	6.0	2.6	4.2	5.471	1,599
Propane	$2.25/ gal	$ 722.43	1.8	2.9	1.3	2.0	6.31	1,844
Electricity	$0.10/ kW-hr	$ 727.68	1.8	2.9	1.3	2.0	11.4	2,831
Heat Pump	COP = 2.5	$ 291.07	4.5	7.2	3.1	5.1	11.4	1,132
#2 Fuel Oil	$2.25/ gal	$ 479.86	2.7	4.4	1.9	3.1	7.3	2,133

Table 7-6 emphasizes the fact that a solar heating system is a better investment for some households than others, depending primarily on the backup heat source. It also demonstrates that external financial incentives can be a deal maker/breaker. For the Goldade Household, which uses Natural Gas, the SPP = 3.7 years, and if a 30% utility financial inducement had been available the SPP would have been 2.6 years. However, for a family that winter heats with propane, the SPP_{NL} =1.8 years, so even without external incentives the solar heating investment is an excellent investment for some Northern Nevada consumers.

Table 7-6 reveals the yearly savings due to solar heating are substantial. However, these values do not take into account the cost and emissions of the blower. Over a two year period the total time the blower was in operation was recorded to be 1617 hours. Assuming the blower is operational for 808.5 hours/year and consumes 283 W of power the yearly power consumed is estimated to be 228.8 kWh, which is equivalent to 7.78 Therms. At $0.10/kWh the annual power cost to run the blower is approximately $23, which is small compared to the solar savings. In some installations, where the blower is located inside the heated space, the heat generated from the blower will contribute to satisfying the heating load; as such, the heat is not "lost", whereas if the blower were not located in the heated space this heat would not contribute to the heating load.

To illustrate the extraordinary effectiveness of a SBAC in the Reno area, a similar f-chart analysis was conducted assuming the same collector (A_c, F_R, U_L and β are the same) were installed in Madison, Wisconsin, which has a colder winter and much less insolation than Reno. The heating load is higher. However, the incident $\bar{H}_T$ is much lower in that part of the world, and the savings are less than 1/3 of that estimated from the same configuration installed in Reno! Consequently payback periods will be much longer (by a factor of 3!) in Wisconsin, as a result a solar investment is not as attractive. This emphasizes the uniqueness of the Great Basin Area, and specifically Northern Nevada. By these estimates, should a home owner in Madison install a comparable

SBAC as installed in the Goldade house via a contractor, the collector will fail to pay for itself over its estimated life span, if it is not incentivized.

Three elements are required for a successful solar space heating investment: (1) cold winters; (2) abundant winter insolation; and (3) expensive heating energy. Reno has all three. The system would not be lucrative in Phoenix, which has abundant sunshine but a low winter heating requirement, because it would not be utilized enough days to provide amortization. And Seattle houses, like Madison, needs winter heat but have insufficient sun to operate the system economically over the winter months.

Although the return on investment can be estimated numerically, there are some intangible benefits to winter solar heating. Especially for people who turn the thermostat down when they are absent, there are times when the house will be pleasantly warmer than expected due to a good solar day, particularly during the swing season (October, April, March), but this can be true any heating month. Also, there is a satisfaction to knowing that one is minimizing his/her energy footprint by consuming less fossil fuel. Some people take fulfillment from minimizing the CO_2 produced by consumption of fossil fuel (this will be discussed below).

Carbon Dioxide Mitigation

The national average CO_2 emissions of natural gas burned is 5.471 kg CO_2/therm (U.S. Energy Information Administration, 2015). Since Table 7-6 indicates the Goldade solar system saves 248 Therms/year, the total CO_2 atmospheric reduction attributed to

the solar system is [5.471*248/0.85=] 1599 kg/year = 3520 lb/year. This value and CO_2 saving relevant to other fuels are shown in the last column of Table 7-6. Over an estimated 25-year system lifetime this CO_2 reduction to the atmosphere is 1596*25= 40,000 kg = 88,100 pounds = 44.0 tons, which is significant!

The average yearly net CO_2 savings due to solar heating if electric heating is employed can be estimated by utilizing national average emissions for electricity (11.4 kg CO_2/Therm) (U.S. Energy Information Administration, 2015). Then (248 Therm/year)(11.4 kg CO_2/Therm)= 2827 kg CO_2/year are defrayed from atmospheric discharge. If a heat pump is utilized then 2827/2.5= 1131 kg CO_2/year are avoided from atmospheric introduction.

The significant reduction in CO_2 atmospheric emissions accruing from adoption of solar space heating in itself should interest government and utility planners to promote financial incentives for SBACs. If this information were widely published, then many conscientious people and planners would become more interested in winter solar space heating.

Chapter 8. Summary, Results and Conclusion

- As has been documented in this thesis and other sources, Site Built Air Collectors (SBACs) if properly designed and constructed have appreciable financial and environmental benefits (Beard, 1993), (Kiley, 1992), (Turner, 2015).

- The benefits of these collectors are substantial in the Northern Nevada area, possibly being the most attractive from of renewable energy for this and other high desert locations. Should local incentive grantors support SBACs it is only logical that these collectors would have a prevalent role in most of the Great Basin environment.

- The most probable reason SBACs are not commonplace is because of the uncommon winter conditions in high desert environments in which SBACs are feasible. These conditions naturally make these collectors viable only in niche markets. Consequently, the SBAC market is likely not substantial enough to achieve main stream adoption throughout the country, and support by government agencies.

- SBACs are inherently flexible in design and material usage. This was demonstrated by the Goldade house-hold, in which the collector was largely constructed from past project materials greatly diminishing the cost of the collector. This brings up the

tantalizing prospect of SBACs being entirely constructed from recycled materials, further improving their environmental impact while potentially lowering cost.

- The primary reason incentive grantors are wary of awarding incentives for SBACs is because, currently, there is no way to economically rate a SBAC. The Mobile Solar Evaluation Laboratory (MSEL) has demonstrated that it is feasible to rate SBAC in an expedient and economical manner, with results comparable to those generated by the Solar Rating Certification Corporation (SRCC), the industry standard.

- The MSEL can give incentive grantors confidence in determining and supporting proficient SBACs.

- A trained technician should be able to evaluate at least one solar system per day when weather conditions permit.

- The standards outlined by SRCC and ASHRAE are largely overly complicated and unneeded for real-world field testing of SBACs.

- To further simplify the MSEL, it was demonstrated that a simple hand held velocity meter can render reliable air flowrate measurements relative to Venturi tubes. Therefore the MSEL should feature hand held velocity meters for future use.

- Using theory generated (Duffie & Beckman, 1980), it is possible to reliably estimate the performance of a properly designed SBAC. These estimates can be compared with field tests of the MSEL. Furthermore the same theory allows for year round testing, and applies to collectors that are not oriented normal to the incident solar radiation at the time of the field test. This will allow for year round testing.

- The low cost of the MSEL and speed with which a test can be conducted has the potential to drastically lower the costs associated with certifying all air collectors.

- The Goldade System study proves that owner site built solar systems can be practical and economical. Such systems are worthy of financial incentives, and can considerably reduce carbon emissions to the atmosphere.

- The simple payback period of a SBAC can range from 1.8 years to 6.0 years, without financial inducements, depending on backup heating source and whether or not the homeowner can build the system himself.

- With pecuniary incentives, solar space heating with a SBAC becomes financially practical in Northern Nevada (and likely the rest of the Great Basin).

- By avoiding consumption of fossil fuels, the relatively small Goldade collector reduces 1600 kg (3530 lb) of CO_2 added to the atmosphere each year.

Works Cited

American Society of Heating, Refrigeration, and Air Conditioning Engineers (ASHRAE). (1993). ASHRAE Standard 41.2-1987. *Standard Methods for Laboratory Airflow Measurement*. Atlanta, Georgia, USA: Approved American National Standard.

American Society of Heating, Refrigeration, and Air Conditioning Engineers (ASHRAE). (2010). Standard 93-2010. *Methods of Testing to Determine the Thermal Performance of Solar Collectors*. Atlanta, Georgia, USA: Approved American National Standard.

American Society of Heating, Refrigeration, and Air Conditioning Engineers (ASHRAE). (2001). *ASHRAE Handbook of Fundamentals.* Atlanta, Georgia, USA: Approved American National Standard.

Beard, J. (1993). *Technical and Economic Performance of Site Built Solar Air Heaters.* University of Nevada Reno.

Can-Filters. (2007). *Can Fans RS Series*. (Can-Filters) Retrieved from Can Filters : http://www.canfilters.com/fan_metal_home.html

Cengel, Y., & Turner, R. (2001). *Fundamentals of Thermal- Fluid Sciences.* McGraw-Hill Higher Education.

Clean Energy Authority. (2015). *Nevada Solar Rebates and Incentives*. Retrieved from Clean Energy Authority: http://www.cleanenergyauthority.com/solar-rebates-and-incentives/nevada/

Duffie, J., & Beckman, W. (1980). *Solar Engineering of Thermal Processes.* New York City: Wiley-Intersience Publication.

EVsRoll. (n.d.). *DIY Solar Air Heater Boxes*. Retrieved from instructables: http://www.instructables.com/id/DIY-Solar-Air-Heater-Boxes/

Hernandez, A., & Quinonez, J. (2013). Analytical models of thermal performance of solar air heaters of double-parallel flow and double-pass counter flow. *SciVerse ScienceDirect*(Renewable Energy).

Hoekman, Broch, A., Robbins, C., Jacobson, R., & Turner, R. (2012). *DRI Renewable Energy Center-Final Report.* Reno: Desert Research Institute.

Holman, J. (1984). *Experimental Methods for Engineers.* McGraw-Hill Publishing Co.

Home-Depot. (2015, July). *Shopping: Home Depot*. (Home Depot) Retrieved from Home Depot Website: http://www.homedepot.com

Kiley, M. (1992). *Analysis of a Site Built Active Air Solar Heater.* University of Nevada Reno.

Klein, S. (1979). Calculation of the Monthly-Average Transmittance-Absorptance Product. *23*.

Mother Earth News. (2015). *DIY Solar Heating with the Heat Grabber*. Retrieved from Mother Earth News: http://www.motherearthnews.com/diy/diy-solar-heating-zmaz77sozgoe.aspx

Mowris, E. J. (2010). *California's Solar Water Heating Program: Scaling Up to Install 200,000.* Retrieved from aceee.org: http://aceee.org/files/proceedings/2010/data/papers/2197.pdf

Nevada State Legislator. (2015, February 11). Chapter 701A- Energy-Related Tax Incentives. *Nevada Revised Statutes*. Carson City, Nevada, USA: Nevada State Legislator.

Njomo, D. (1994). *Techno-Economic Analysis of a Platic Cover Solar Air Heater.* Univerisy of Yanunde.

NV Energy. (2015). *SolarGenerations Heating*. Retrieved from NV Energy: https://www.nvenergy.com/renewablesenvironment/renewablegenerations/solarwater/incentives.cfm

Pahl, G. (2003, October). *A History of Solar Water Heating*. Retrieved from mother earth news: http://www.motherearthnews.com/renewable-energy/history-of-solar-water-heating-zmaz03onzgoe.aspx

Perlin, J. (2015). *California Solar Center*. Retrieved from Solar Thermal History: http://californiasolarcenter.org/history-solarthermal/

Rogers, P., Fuller, R., & Luther, M. (2007). *Prefromace of a 120 sqr Meter Solar Air Heater for a Commerical building in Victoria.* Australian and New Zealand Solar Energy Society .

Solar Components Corporation. (2015). Technical Summary. Manchester.

Solar Rating & Certification Corporation. (2014, July 15). SRCC Standard 100-2014-07. *Minimum Standards for Solar Thermal Collectors*. Cocoa, Florida, USA: Solar Rating & Certification Corporation.

Solar Rating & Certification Corporation. (2015). *Apply For Certification*. Retrieved from solar-rating.org: http://www.solar-rating.org/apply/index.html

South West Gas. (2015). *Nevada Smarter Greener Better Solar Water Heating Program*. Retrieved from South West Gas: http://www.swgasliving.com/rebates/nevada/nevada-smarter-greener-better%C2%AE-solar-water-heating-program-business

Temple & Adams. (1980). *Solar Heating - A Construction Manual.* Chilton Book Company.

Turner, R. (2015). Personal Communication.

U.S Department of Energy. (2015, July). *Nevada Solar Air Collector Programs*. Retrieved from Database of State Incentives for Renewables & Efficiency: http://programs.dsireusa.org/system/program?state=NV

U.S. Energy Information Administration. (2004, April 02). *Greenhouse Gases, Climate Change, and Energy*. Retrieved from U.S. Energy Information Administration: http://www.eia.gov/oiaf/1605/ggccebro/chapter1.html

U.S. Energy Information Administration. (2015, June 18). *Frequently Asked Questions*. (U.S. Energy Information Administration) Retrieved from U.S. Energy Information Administration Web Site: https://www.eia.gov/tools/faqs/faq.cfm?id=73&t=11